Soil Dynamics and Earthquake Engineering 35 (2012) 41–58

Contents lists available at SciVerse ScienceDirect

Soil Dynamics and Earthquake Engineering

journal homepage: www.elsevier.com/locate/soildyn

A new methodology to determine elastic displacement spectra in the near-fault region

Ch.A. Maniatakis, C.C. Spyrakos *

Laboratory for Earthquake Engineering, Department of Civil Engineering, National Technical University of Athens, Zografos, Athens 15700, Greece

ARTICLE INFO

Article history:
Received 10 May 2010
Received in revised form
18 October 2011
Accepted 18 October 2011
Available online 3 December 2011

ABSTRACT

The evaluation of the displacement demand especially at small distances from the causative fault, in the so-called near-source region, is a subject of particular interest for earthquake engineering design, in the light of the growing application of the displacement-based design philosophy. This study presents a new methodology to determine the elastic displacement spectra using a sample of near-fault records from small-to-moderate magnitude earthquakes, typical of the seismic activity in Europe. The displacement spectrum is developed using near-fault attenuation relationships available in literature for peak ground velocity that is less sensitive in the procedures applied to correct the accelerograms. Also, the distance from the causative fault and the type of directivity are taken into consideration. The prevailing period corresponds to the maxima of the displacement spectra for zero damping and is used to normalize the spectra, leading to significant decrease of the statistical dispersion. The average bi-normalized spectrum, in terms of the peak ground displacement $d_{g,max}$ and the dominant period $T_{d\text{-}p}$, appears to be slightly affected by the soil category and earthquake magnitude. A correlation between the damping correction factor η and the normalized period $T/T_{d\text{-}p}$ is detected and the applicability of several provisions of the current version of Eurocode 8 is examined, including characteristic periods and spectral amplitudes.

1. Introduction

The growing application of displacement-based design in earthquake engineering urges for a reliable determination of the displacement demand, especially at distances close to causative faults, where the structural damage is usually most severe, as recent seismic activity has revealed [1–4]. Unlike the conventional force-based philosophy where the primary interest is the design of structural members to withstand a set of forces at the plastic limit, the Direct Displacement-Based Design (DDBD) is based on a single-degree-of-freedom (SDOF) representation of a structure at peak displacement response. A displacement spectrum is needed to determine the effective period of this SDOF system [5]. The determination of the displacement spectrum for a wide range of damping ratio values ξ is also valuable to perform pushover analysis and assess the performance of existing structures [6]. In the present research an evaluation of Eurocode 8 [7] provisions for the displacement spectrum is performed based on a dataset of near-fault seismic records. Current provisions are found to have significant shortcomings, which are discussed in light of a new methodology. Emphasis is given on small-to-moderate earthquake magnitudes, which are more common in Europe. It should be noted that EC8 design spectrum is defined regardless of the distance from the source and rupture direction and differentiates only for two earthquake magnitude ranges: (1) Spectrum Type 1 valid for $M_S \geq 5.5$, and (2) Spectrum Type 2 valid for $M_S < 5.5$. Several studies led to the final version of EC8 design spectrum, i.e., [8,9].

Bommer and Elnashai [10] have examined the displacement spectra *SD* of several seismic codes from various countries that result from the acceleration spectrum values *SA* for all periods *T* with application of the relationship

$$SD(T) = SA(T)\left[\frac{T}{2\pi}\right]^2 \quad (1)$$

and have concluded that the spectra obtained in this way lead to non-realistic spectral values at long periods, since characteristic periods only for the constant accelerations region were predicted, according to the design concepts of that time. They calculated displacement spectra using attenuation relationships and proposed a new design spectrum that depends on the earthquake magnitude and soil conditions. Displacement spectra for several values of damping ratio based on attenuation relationships have also been presented by Tolis and Faccioli [11], who proposed also the introduction of the characteristic period T_E denoting the end of the constant spectral displacement region. Bommer et al. [12]

* Correspondence to: Laboratory for Earthquake Engineering, School of Civil Engineering, National Technical University of Athens, Zografos, Athens, 15700, Greece. Tel.: +30 2107721187; fax: +30 2107721182.
E-mail address: cspyrakos@central.ntua.gr (C.C. Spyrakos).

0267-7261/$ - see front matter © 2011 Published by Elsevier Ltd.
doi:10.1016/j.soildyn.2011.10.005

suggested the following period-independent expression for damping correction or scaling factor η adopted from current EC8 [7]:

$$\eta(\xi) = \frac{SD(T,\xi)}{SD(T,\xi=5\%)} = \sqrt{\frac{10}{(5+\xi)}} \quad (2)$$

where $SD(T,\xi)$ is the spectral displacement, T is the period and ξ is the damping ratio.

Several studies have shown that the current EC8 provisions might overestimate the spectral displacement values and proposed modification of the spectral corner periods [13,14]. It has been observed that time histories of similar peak ground acceleration values can have significantly different spectral displacement values at large periods [15]. This observation is in agreement with the opinion that different mechanisms are responsible for the low and high frequency contents of strong ground motion [16,17]. The need to normalize the period of response spectra in terms of the dominant period of motion, even though suggested by several researchers, i.e., [18–21] has not yet been adopted by current seismic design codes mostly because of the ambiguity regarding the determination of the dominant period.

The characteristics of displacement spectra at long periods were examined by Faccioli et al. [22], who used simple wavelets to formulate simple analytical expressions for displacement spectra accounting for the effects of near-fault phenomena, magnitude, distance from the source and soil conditions. The critical role of filtering in maintaining the long-period spectral content and the inappropriateness of magnitude-independent corner periods have been revealed by the recently proposed European predictive equations for displacement response spectra [23,24]. According to the results of these studies the constant scaling factor proposed in EC8 should be considered as adequate for periods up to 6–7 s, while overestimation of spectral values, especially at small periods, has been detected, as has already been shown by other researchers, i.e., [13,14].

Based on the studies that have preceded the formation of the current Eurocode 8 spectrum, one can conclude that the major problems that can be identified are

i. application of different correction procedures that can have a significant impact on strong motion time histories;
ii. errors from the statistical processing of a large number of records with different frequency content characteristics;
iii. difficulty of a reliable peak ground displacement $d_{g,max}$ estimation;
iv. difficulty in determining the corner period of displacement spectra.

The scope of this study is twofold: (i) propose a methodology that determines the elastic displacement spectra in the area near the causative fault of small-to-moderate magnitude earthquakes and (ii) assess whether the current EC8 displacement spectrum can adequately account for near-source phenomena. The proposed methodology attempts to overcome the major problems of the displacement spectrum determination stated above. The displacement spectrum is expressed in a standard and in a bi-normalized form, adopting a determination of the dominant period of strong ground motion that is based on Fourier analysis. Attenuation relationships for near-fault motion are employed to identify the spectral amplitude. The spectral demand is finally estimated based on peak ground velocity rather than the peak ground displacement, which is usually sensitive to the correction procedures applied.

2. Selection of earthquake records

Small-to-moderate magnitude earthquake records are selected, including near fault seismic excitations from Greece, the country with the most intense seismic activity in Europe. Earthquake events with magnitude $M_W > 6.5$ are quite rare for European countries. Common engineered structures present modal characteristics within the prevailing frequency content of this range of magnitudes, which constitutes a profound reason of selecting these events. However, some representative records of slightly greater magnitude have been included, i.e., two records from the 1981 Corinth, Greece (Alkyonides) earthquake with $M_W=6.7$ and ten records from the 1979 Imperial Valley earthquake with $M_W=6.5$.

The earthquake ground motion is obtained from the PEER strong-motion database [25] and the strong-motion database of the Institute of Engineering Seismology and Earthquake Engineering (ITSAK) [26]. The database used is representative of shallow crustal seismic events. Most of the selected Greek earthquake records satisfied a series of damage potential criteria established to characterize strong ground motion: the frequency content, the energy content, the amplitude and the duration [27]. A number of smaller magnitude records are also included to enrich the sample in the range of moment magnitude $M_W < 5.5$, with epicentral distance $R_{epi} \leq 25$ km and peak ground acceleration $a_g \geq 50$ cm/s^2. In addition to the Greek earthquake records, records from the following five events were included: the 1966 Parkfield earthquake with $M_W=6.2$, the 1979 Imperial Valley earthquake with $M_W=6.5$, the 1979 Coyote Lake earthquake with $M_W=5.7$, the 1984 Morgan Hill earthquake with $M_W=6.2$ and the 1987 Whittier Narrows earthquake with $M_W=6.0$. The final development of the earthquake sample is based on the following criteria:

1. The sample should include sufficient records of small-to-moderate earthquakes with a magnitude in the range of $5.5 \leq M_W \leq 6.5$ considering the fact that: (i) different spectra are valid for earthquake prone areas for moment magnitude $M_S \geq 5.5$ according to Eurocode 8, and (ii) seismic events with $M_W \geq 6.5$ are rare for most European countries.
2. Records from a variety of epicentral (R_{epi}) or Joyner–Boore (R_{jb}) distances with strong motion characteristics in the near-fault region were selected. The near-fault records from a previous study were included [27], in addition to the records from Greek seismic events with an R_{epi} smaller than 25 km and a peak ground acceleration a_g equal to at least 50 cm/s^2. For the PEER database the R_{jb}, which is the shortest horizontal distance from the recording site to the vertical projection of the rupture, is selected to be smaller than 20 km.
3. Records from PEER with different angles between the site and the fault plane were selected, in order to be representative of both forward and backward types of directivity [28].
4. In order to study the effects of the geotechnical conditions, records for a variety of soil conditions were selected. According to the USGS classification used by the PEER database, each ground type is characterized by the average shear wave velocity $V_{S,30}$ in the upper 30 m of the soil: ground type A is characterized by $V_{S,30} > 750$ m/s, ground type B is characterized by 360 m/s $< V_{S,30} <$ 750 m/s, ground type C is characterized by 180 m/s $< V_{S,30} <$ 360 m/s and ground type D is characterized by $V_{S,30} <$ 180 m/s, a categorization that is equivalent to the soil classification according to EC8 [7], which is available for the Greek earthquake records.

The selected records listed with ascending moment magnitude are shown in Table 1. Filtering details for the worldwide near-fault records are available at the PEER site. The procedures

Table 1
Near-fault records used in the present study.

Event	Date	Magnitude		No.	Record name	Orientation	Soil type					$R_{epicentral}$	PGA	PGV	PGD	Fault rupture length (km)	Fault rupture width (km)	Cut-off frequency	$T_{v\text{-}p}$ (s)	$T_{d\text{-}p}$ (s)
		M_W	M_S				Geomatrix			USGS	EC8	(km)	(cm/s^2)	(cm/s)	(cm)			fcoff (Hz)		
							1	2	3											
Pyrgos	03/26/93	4.9		1	PYR19306.V2	N351°					C	6.0	105.6	4.3	0.29			0.701	0.28	0.44
Preshock		4.9		2	PYR19306.V2	N261°					C	6.0	221.5	6.3	0.46			0.701	0.28	0.28
Kremydia (S.Greece) aftershock	10/25/84	5.0		3	PEL18401.V2	N280°					A	9.0	166.6	9.0	0.58			0.394	0.28	0.76
		5.0		4	PEL18401.V2	N190°					A	9.0	172.7	7.9	0.58			0.394	0.30	0.86
Kozani aftershock	05/19/95	5.1		5	KRR19501.V2	N69°					B	12.0	185.3	15.3	1.34			0.300	0.94	0.94
		5.1		6	KRR19501.V2	N339°					B	12.0	262.0	14.7	1.26			0.300	0.40	0.40
	05/15/95	5.1		7	CHR19513.V2	N90°					B	13.0	157.0	4.5	0.19			0.300	0.16	0.76
		5.1		8	CHR19513.V2	N0°					B	13.0	132.1	3.8	0.16			0.300	0.18	0.64
	05/17/95	5.3		9	CHR19532.V2	N90°					B	11.0	116.7	4.3	0.32			0.300	0.36	0.56
		5.3		10	CHR19532.V2	N0°					B	11.0	130.4	4.7	0.45			0.300	0.22	0.46
Kalamata	09/15/86	5.3		11	KAL18608.V2	N180°					B	3.0	232.8	22.7	2.79			0.205	0.76	0.76
Aftershock		5.3		12	KAL18608.V2	N90°					B	3.0	137.1	8.1	0.99			0.205	0.60	1.38
Cephalonia	03/24/83	5.4		13	ARG18308.V2	N59°					B	22.0	240.1	6.4	0.22			0.872	0.16	0.44
Aftershock		5.4		14	ARG18308.V2	N329°					B	22.0	285.3	9.9	0.35			0.872	0.18	0.50
		5.4		15	PYR19308.V2	N261°					C	14.0	425.8	20.7	2.40			0.307	0.36	0.72
Patras	07/14/93	5.6		16	PAT19302.V2	N150°					C	10.0	143.7	8.4	0.89			0.393	0.42	0.74
		5.6		17	PAT19302.V2	N60°					C	10.0	192.5	10.3	1.29			0.393	0.70	0.70
		5.6		18	PAT29302.V2	N110°					C	9.0	164.2	9.3	0.77			0.283	0.42	1.00
		5.6		19	PAT29302.V2	N20°					C	9.0	388.6	8.5	0.89			0.283	0.12	1.14
Konitsa	8/5/1996	5.7		20	KON19601.V2	N90°					B	8.0	168.4	29.1	7.60			0.250	0.86	0.86
		5.7		21	KON19601.V2	N0°					B	8.0	168.4	14.5	1.90			0.250	0.86	0.86
		5.7		22	KON29601.V2	N90°					C	8.0	383.7	20.8	2.49			0.150	0.50	0.66
Coyote	8/6/1979	5.7	5.6	23	COYOTELK CY	160°	H	F	A		A	8.0	154.0	10.8	1.31	6.6	7.0	0.200	0.54	2.20
Lake		5.7	5.6	24	COYOTELK CY	250°					A	8.0	273.7	20.3	2.33	6.6	7.0	0.200	0.42	0.64
		5.7	5.6	25	COYOTELK G01	230°	I	F	A	A	A	12.6	101.0	3.4	0.48	6.6	7.0	0.250	0.20	2.32
		5.7	5.6	26	COYOTELK G01	320°					A	12.6	129.5	8.2	1.52	6.6	7.0	0.250	0.20	2.00
Coyote	8/6/1979	5.7	5.6	27	COYOTELK G02	50°	I	Q	D	C	C	10.9	207.0	10.9	2.29	6.6	7.0	0.200	0.98	1.70
Lake		5.7	5.6	28	COYOTELK G02	140°					C	10.9	332.6	24.9	5.81	6.6	7.0	0.200	0.90	1.54
		5.7	5.6	29	COYOTELK SJ3	67°	I	Q	D	B	B	23.9	95.2	5.9	0.55	6.6	7.0	0.230	0.62	0.62
Lefkas	11/4/1973	5.8		30	LEFA7301.V2	L					C	23.7	490.8	46.5	4.94			0.754	0.78	0.92
		5.8		31	LEFA7301.V2	T					C	23.7	234.2	20.9	2.30			0.754	0.82	0.82
Athens	9/7/1999	5.9		32	ATH29901.V2	N36°					B	19.6	108.1	5.1	0.48			0.400	0.38	1.20
		5.9		33	ATH29901.V2	N306°					B	19.6	155.6	6.9	1.09			0.400	0.22	1.58
		5.9		34	ATH39901.V2	N46°					B	15.3	258.6	16.1	1.87			0.200	0.70	0.70
		5.9		35	ATH39901.V2	N316°					B	15.3	297.2	14.7	2.12			0.200	0.22	2.46
		5.9		36	ATH49901.V2	N70°					A	16.6	118.6	8.9	0.90			0.300	0.42	0.92
		5.9		37	ATH49901.V2	N340°					A	16.6	107.9	8.5	1.88			0.300	1.32	1.32
		5.9		38	ATHA9901.V2	L					C	18.6	82.0	5.3	1.43			0.125	0.48	1.82
		5.9		39	ATHA9901.V2	T					C	18.6	99.7	7.4	1.36			0.125	0.24	1.48
		5.9		40	SGMA9901.V2	L					C	17.2	145.9	12.7	2.91			0.125	0.52	2.64
		5.9		41	SGMA9901.V2	T					C	17.2	234.5	13.4	1.57			0.125	0.22	0.94
		5.9		42	SPLB9901.v2	N320°					B	13.8	318.3	21.5	2.50			0.125	0.18	1.28
		5.9		43	SPLB9901.v2	N50°					B	13.8	306.3	18.9	3.56			0.125	0.24	5.16
Whittier	10/1/1987	6.0	5.7	44	WHITTIER A-ALH	180°	A	Q	D	B	B	6.8	326.7	22.0	2.42	10.0	6.0	0.300	0.24	1.16
Narrows		6.0	5.7	45	WHITTIER A-ALH	270°					B	6.8	406.1	16.3	2.32	10.0	6.0	0.300	0.38	0.76

Table 1 (*continued*)

Event	Date	Magnitude		No.	Record name	Orientation	Soil type					$R_{epicentral}$	PGA	PGV	PGD	Fault rupture length (km)	Fault rupture width (km)	Cut-off frequency	$T_{v\text{-}p}$ (s)	$T_{d\text{-}p}$ (s)
		M_W	M_S				Geomatrix			USGS	EC8	(km)	(cm/s^2)	(cm/s)	(cm)			fcoff (Hz)		
							1	2	3											
		6.0	5.7	46	WHITTIER A-OBR	270°	A	Q	D		B	9.1	441.5	16.0	2.18	10.0	6.0	0.400	0.18	0.98
		6.0	5.7	47	WHITTIER A-OBR	360°					B	9.1	392.4	22.9	2.53	10.0	6.0	0.400	0.20	0.86
		6.0	5.7	48	WHITTIER A-W70	0°	A	H	D	B	B	20.9	194.2	4.8	0.16	10.0	6.0	0.200	0.58	0.96
		6.0	5.7	49	WHITTIER A-W70	270°					B	20.9	148.1	2.2	0.09	10.0	6.0	0.200	0.22	1.26
		6.0	5.7	50	WHITTIER A-LUR	90°	B	H	D	C	C	10.7	353.2	9.8	0.92	10.0	6.0	0.300	0.18	0.98
		6.0	5.7	51	WHITTIER A-LUR	180°					C	10.7	345.3	18.1	2.35	10.0	6.0	0.300	0.70	0.70
Kalamata	09/13/86	6.0		52	KAL18601.V2	N180°					B	12.3	229.3	30.9	7.10			0.291	0.62	1.94
		6.0		53	KAL18601.V2	N90°					B	12.3	263.9	24.0	5.56			0.291	0.66	1.46
		6.0		54	KALA8601.V2	L					B	12.3	217.0	32.9	7.68			0.200	1.14	1.14
		6.0		55	KALA8601.V2	T					B	12.3	291.3	32.4	6.42			0.200	0.66	1.30
Parkfied		6.2		56	PARKF C05	85°	I	P	B	C	C	32.6	52.0	4.6	2.11	24.9	12.0	0.200	2.70	2.70
Morgan Hill	4/24/1984	6.2	6.1	57	MORGAN AND	250°	I	Q	D	B	B	16.7	415.0	25.3	4.59	27.0	11.5	0.100	0.52	2.46
		6.2	6.1	58	MORGAN AND	340°					B	16.7	283.5	27.6	6.35	27.0	11.5	0.100	0.70	0.72
		6.2	6.1	59	MORGAN G04	360°					B	37.3	341.4	17.4	3.12	27.0	11.5	0.100	0.52	1.02
		6.2	6.1	60	MORGAN G06	90°					B	37.3	286.5	36.7	6.13	27.0	11.5	0.100	1.10	1.10
Lefkas	08/14/2003	6.2		61	LEF10301.V2	N65°					C	12.0	333.4	14.7	2.75			0.100	0.52	1.54
		6.2		62	LEF10301.V2	N335°					C	12.0	408.6	15.7	5.08			0.100	0.62	0.62
Aegion	06/15/95	6.4		63	AIGA9501.V2	L					B	21.6	484.3	43.5	7.53			0.350	0.42	1.98
		6.4		64	AIGA9501.V2	T					B	21.6	507.2	43.9	4.50			0.350	0.48	0.48
Imperial Valley	10/15/1979	6.5	6.9	65	IMPVALL H-AEP	45°	I	Q	D	C	C	2.5	320.8	42.8	10.26	50.0	13.0	0.050	1.58	1.60
		6.5	6.9	66	IMPVALL H-AEP	315°					C	2.5	255.1	24.8	3.59	50.0	13.0	0.050	0.28	1.14
		6.5	6.9	67	IMPVALL H-AGR	3°	I	Q			C	2.6	363.0	35.4	10.02	50.0	13.0	0.050	0.54	1.86
		6.5	6.9	68	IMPVALL H-AGR	273°					C	2.6	216.8	42.2	11.71	50.0	13.0	0.050	0.56	1.90
		6.5	6.9	69	IMPVALL H-EMO	0°	I	Q	D	C	C	19.4	308.0	71.8	25.59	50.0	13.0	0.100	0.78	2.58
		6.5	6.9	70	IMPVALL H-EMO	270°					C	19.4	290.4	90.4	31.65	50.0	13.0	0.100	2.66	3.14
		6.5	6.9	71	IMPVALL H-E06	140°	I	H	D	C	C	27.5	402.2	64.9	27.57	50.0	13.0	0.100	2.54	2.58
		6.5	6.9	72	IMPVALL H-E07	230°					C	27.5	454.2	109.3	44.72	50.0	13.0	0.100	3.72	3.76
		6.5	6.9	73	IMPVALL H-SHP	0°	A	Q	C	C	C	12.4	281.5	19.4	2.64	50.0	13.0	0.200	0.20	2.28
		6.5	6.9	74	IMPVALL H-SHP	270°					C	12.4	496.4	31.0	5.47	50.0	13.0	0.200	0.54	0.72
Korinthos (Alkyonides)	02/24/1981	6.7		75	KORA8101.V2	L					C	32.0	229.5	22.7	3.52			0.413	0.54	1.64
		6.7		76	KORA8101.V2	T					C	32.0	274.4	17.7	2.57			0.413	0.42	1.40

proposed by Margaris [29] and Skarlatoudis et al. [30] have been applied to correct and filter the available Greek strong motion records. A filter cut-off frequency f_{coff} ($1/T_{coff}$), different for each record, was selected to eliminate the noise, which in some cases is rather high as shown in Table 1. Currently a new strong motion data processing technique is applied for the records obtained by the Greek accelerographic networks for the derivation of new ground motion prediction equations [31]. However, this procedure has not been completed yet. For this reason spectral values are computed up to 4 s for standard spectra.

3. Estimation of dominant period for the near-fault records.

The extensive research in the seismic response of structures under near-fault seismic excitations demonstrates the importance that researchers attribute directly or indirectly to the dominant period of ground motion, whose role has not been evaluated so far by the current seismic codes. The directivity pulse, more profound in the strike-normal direction of the velocity time history [16,28,32], is the cumulative effect of almost simultaneous arrival of seismic waves at a site towards which a seismic fault ruptures. The period of the pulse has been proved to be one of the most important characteristics of strong motion in the near-fault area [20].

Today, it is believed that the shape of the spectrum is a function of distance from the source, the magnitude of the earthquake, the soil conditions and the wave propagation phenomena, and that the form of the spectrum is significantly affected by the frequency content of ground motion.

Investigations on the response of structures in the near-fault region have shown that the representation of the strong motion in the form of time-history is more realistic than the form of response spectra, e.g., [33–35]. Use of time histories is preferable because a frequency domain representation, such as the response spectra, implies a stochastic process characterized by a uniform distribution of energy throughout the course of motion [33]. In the case of near-fault seismic excitations, energy is concentrated in only a few number of cycles, which are often characterized by a dominant frequency, especially towards the direction at which the rupture is developed [33].

The investigation of characteristics of near-source excitations (amplitude, duration, frequency and energy content) is often done by considering simplified pulse models. This simulation facilitates the quantification of the various parameters in the near fault region, one of which is the period of the dominant pulse. Several different analytical models have been proposed in literature to represent a particular near-fault ground motion (e.g., triangular, rectangular or harmonic functions). The research of Makris [36], Krawinkler and Alavi [34] and Sasani and Bertero [35] has shown that simplified representations of the directivity pulse can describe with sufficient accuracy some of the most salient features of this type of ground motion with pulse-type characteristics.

The definition of the pulse period T_V is given using either the zero crossing time or the time at which the velocity is equal to 10% of the maximum pulse velocity. This definition includes a degree of uncertainty, which can lead to different estimates of T_V. Krawinkler and Alavi [34] defined the pulse period as the period $T_{v\text{-}p}$ that corresponds to the maximum value of the velocity response spectra, a definition usually referred to in the literature, e.g., [37]. In the case of ground motion that is characterized by a single velocity pulse, these different definitions of pulse period provide practically the same results, which is not the case for more complex excitations.

Another common procedure to estimate the characteristics of strong motion in the near-fault region is the use of wavelets. Through wavelet analysis simulation of directivity pulse, Mavroeidis and Papageorgiou [17] concluded that in many cases, the directivity pulse period is much larger than the dominant period of the velocity response spectrum. In a subsequent research, Mavroeidis et al. [20] examined the elastic response of single-degree-of-freedom systems when excited with near-fault motion using a four parameter comprehensive wavelet model, showing that the pulse period is the most influential parameter that differentiates the range of the response.

In the wavelet analysis proposed by Baker [38] signal processing is performed to isolate the dominant pulse of the near-fault motion. When the pulse is significantly large, compared with the remaining time history, the original excitation is characterized as pulse type and the period of the identified pulse is determined. As there is no well defined period for wavelets, since they include a bandwidth of frequencies, Baker uses the period related to the maximum Fourier spectrum amplitude of the resulting wavelet.

Other methods are also available in the literature to determine the predominant pulse period, including non-linear optimization of curve fitting using sine waves or graphical evaluation, e.g., [39,40]. However, these methods include uncertainties associated with the user's judgment.

As previously mentioned, the most common alternative method to determine the pulse period is to use the period associated with the maximum value of velocity spectra. Comparison of different approaches has led to the conclusion that the dominant period based on waveform T_p (or T_v) is generally equal to or greater than $T_{v\text{-}p}$ derived from the velocity spectra [37]. In cases where the two periods differ significantly, the period T_v appears to be more reliable. The period $T_{v\text{-}p}$ is associated with a high frequency part of the ground motion, while T_v is related to the period of the distinguishable velocity pulse, as was clearly shown for the Yermo Fire Station earthquake record of the 1992 Landers earthquake by Baker [38].

In light of this controversy regarding the definition of the dominant pulse period, the need for a conclusive mathematical method to determine the frequency range of the velocity pulse in the near-fault area is obvious. In the present research, the dominant period of the velocity pulse is determined based on Fourier analysis according to the methodology proposed by Taflampas [41].

It has already been proved by Hudson [42] that the zero damping pseudovelocity spectrum $SV(\xi=0,\omega_n)$ for each frequency ω_n is an upper bound of the Fourier amplitude spectrum of ground acceleration $FSA(\Omega)$. Consequently, it is likely that the $T_{v\text{-}p}$ period corresponds simultaneously to the maximum value of the $SV(\xi=0,\ \omega_n)$ and the $FSA(\Omega)$ spectra revealing the harmonic component of ground acceleration with the maximum participation at the original wave. Notice that Ω represents ground frequency component while ω_n represents oscillator frequency. Thus, $T_{v\text{-}p}$ is the dominant period of the ground acceleration, which is not necessarily equal to the velocity pulse period. The acceleration time history often contains harmonic components with high frequency that cannot be identified deterministically, while the distinguishable pulse of velocity time history is related to the propagation phenomena in the near-fault region [17].

A similar relationship between the zero damping displacement spectrum $SD(\xi=0,\ \omega_n)$ and the Fourier amplitude spectrum of ground velocity $FSV(\Omega)$ has been proposed by Taflampas [41], who proved that the Fourier amplitude spectrum $FSV(\Omega)$ of ground velocity can be estimated according to the following expression:

$$FSV(\Omega)=\frac{1}{\Omega}\sqrt{\left[\int_0^T a(t)\sin(\Omega t)dt\right]^2+\left[\int_0^T a(t)\cos(\Omega t)dt\right]^2} \tag{3}$$

where T is the total duration and $a(t)$ is the ground acceleration. Assuming that the maximum relative displacement occurs at time

t_d, the spectral displacement of an undamped SDOF oscillator can be calculated from, e.g., [43]:

$$SD(\xi=0,\omega_n)=\frac{1}{\omega_n}\sqrt{\left[\int_0^{td}a(\tau)\sin(\omega_n\tau)d\tau\right]^2+\left[\int_0^{td}a(\tau)\cos(\omega_n\tau)d\tau\right]^2} \quad (4)$$

Comparing Eqs. (4) and (3), it is evident that the Fourier amplitude spectrum for the ground velocity $FSV(\Omega)$ is equivalent to the displacement response spectrum SD for zero damping. Consequently, the dominant period of the velocity pulse can be defined from the frequency $\omega_{d\text{-}p}$ or the period $T_{d\text{-}p}$ that corresponds to the maximum value of zero damping displacement spectra [41].

This mathematical proof both allows an undemanding and concise estimation of the predominant period and explains the difference already described in literature between the period $T_{v\text{-}p}$, which is associated with a high-frequency part of the motion, and the actual period of the pulse T_v. In the following, the adequacy of a single pulse period consideration is examined.

In Fig. 1 the acceleration, velocity and displacement response spectra for the 0^0 component of the record obtained at the Erzincan station from the 1992 Erzincan earthquake at Turkey (M_W=6.6) are shown. The similarity between the acceleration Fourier amplitude spectra $FSA(\Omega)$ and velocity response spectra $SV_{(T,\xi=0\%)}$ can be noticed in Fig. 1(b). Correspondingly, the similarity between the velocity Fourier amplitude spectra $FSV(\Omega)$ and the displacement response spectra $SD_{(T,\xi=0\%)}$ can be observed in Fig. 1(c). The dominant period of the velocity spectrum is $T_{v\text{-}p}$=2.28 s and the dominant period of the displacement spectrum is $T_{d\text{-}p}$=3.05 s. The harmonic components that correspond to $T_{v\text{-}p}$ and $T_{d\text{-}p}$ periods are shown in Fig. 2(a), after applying the Discrete Fourier Transform on the ground velocity time-history. It is clear that the harmonic component corresponding to $T_{d\text{-}p}$ cannot represent the dominant part of the strong motion alone.

In order to represent the significant part of the velocity time history a range of frequencies must be taken into account. This observation, typical for the Fourier analysis concept, even though not well understood in earthquake engineering, explains the applicability of wavelet analysis. There is a need to include a range of frequencies to build the significant part of velocity time history. When all the harmonic components between 0.33 Hz and 0.44 Hz (2.28 s $\le T \le$ 3.05 s) are included a better representation of the time history is achieved, as shown in Fig. 2(b). However, the period $T_{d\text{-}p}$ is the mathematically determined dominant period of the velocity time history [41] and indicates the range of the harmonic components that should be considered as significant for strong ground motion. In the following, the period $T_{d\text{-}p}$ is used to examine the nature of the displacement response spectrum in the near-fault region.

4. Displacement response spectrum characteristics.

4.1. Evaluation of displacement sensitive region of design spectrum

For the reasons outlined above, the dominant period $T_{d\text{-}p}$ is calculated from the period that corresponds to the maximum value of spectral displacement for damping ξ=0%. In the following, the period $T_{d\text{-}p}$ is compared with the dominant period of the pulse T_V, which is calculated from the following relationship proposed by Bray and Rodriguez-Marek [37] that is based on a sample of near-fault records with forward-directivity characteristics and moment magnitude range M_W=6.1–7.6:

$$\ln(T_V)=-5.60+0.93M_W \quad (5)$$

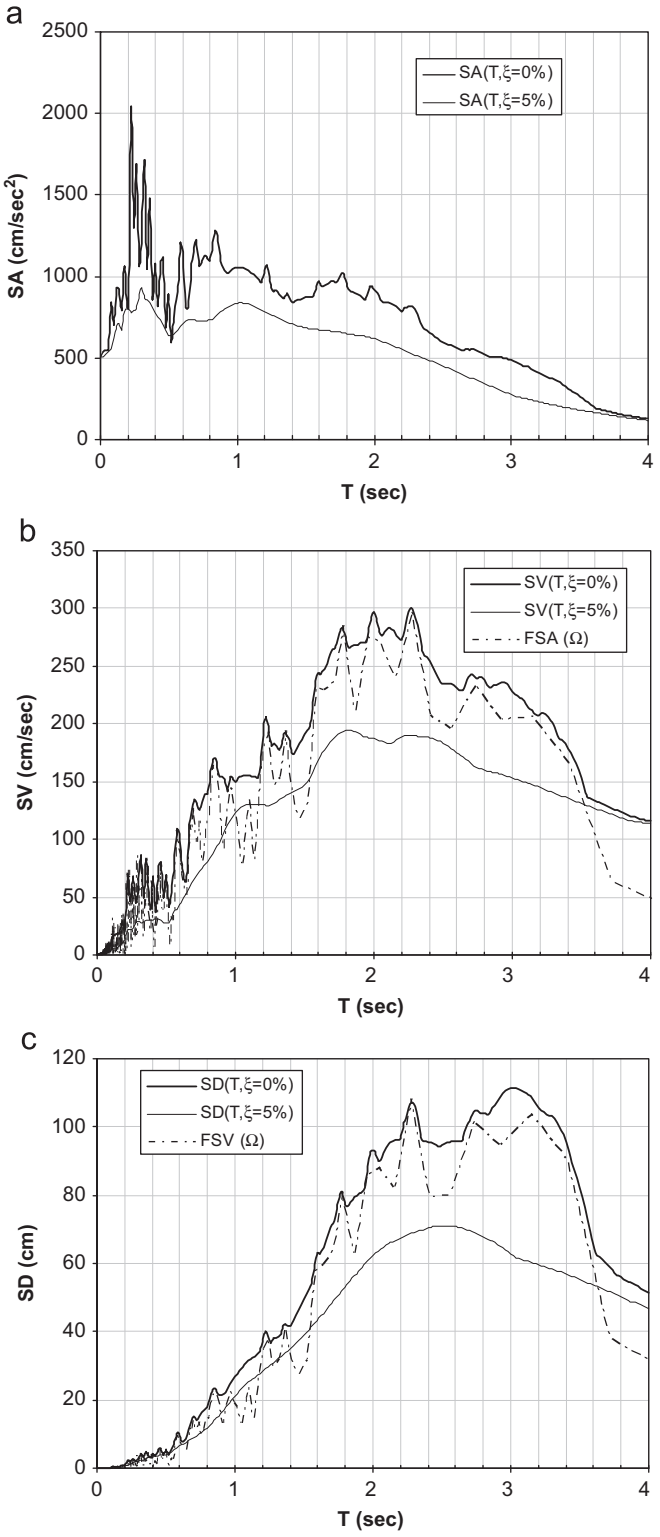

Fig. 1. Response spectra and Fourier amplitude spectra for 1992 Erzincan, Turkey earthquake (M_W=6.6)—Station Erzincan—Comp 000: (a) acceleration response spectrum, (b) velocity response and Fourier amplitude spectra and (c) displacement response and Fourier amplitude spectra.

The application of Eq. (5) for seismic events of smaller magnitude is evaluated. The total dispersion σ_{total} related to the assessment of the velocity pulse period T_v for soil conditions is σ_{total}=0.58.

The evaluation of T_V involves the identification of the number of equivalent half-cycles of pulse motion directly from the

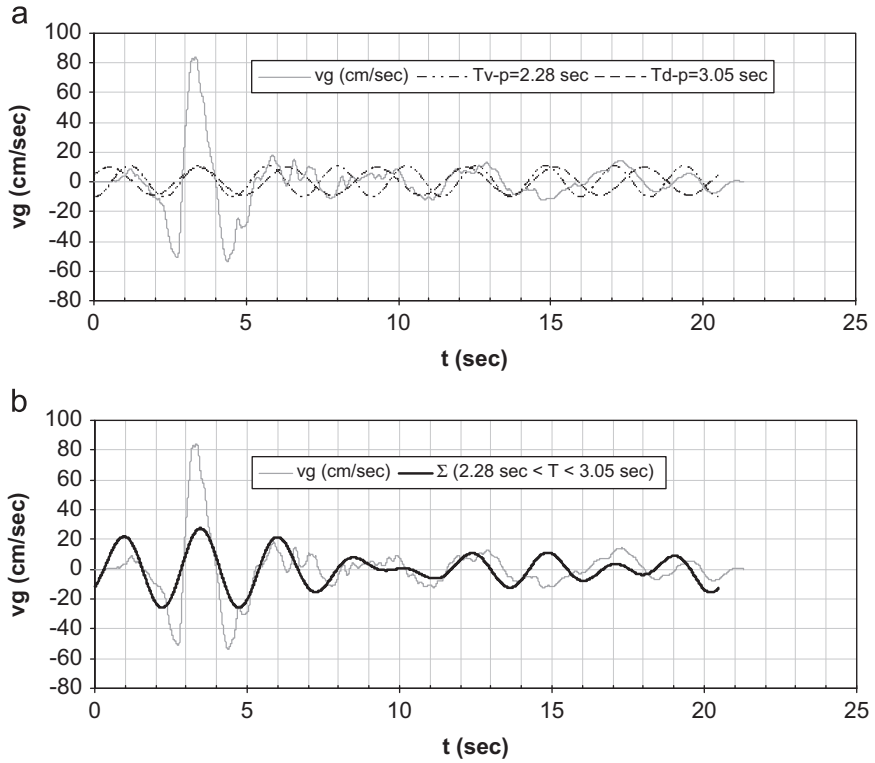

Fig. 2. Fourier analysis for velocity time history of 1992 Erzincan, Turkey earthquake (M_W=6.6)—Station Erzincan—Comp 000: (a) harmonic components for $T_{v\text{-}p}$=2.28 s and $T_{d\text{-}p}$=3.05 s and (b) combination of harmonic components between 0.33 Hz and 0.44 Hz (2.28 s ≤ T ≤ 3.05 s).

velocity time history by comparing it with simple wavelets in order to specify the period of each wavelet half-cycle and its corresponding amplitude. The period of the pulse with the largest amplitude is denoted as T_V. This definition of pulse period uses either zero crossing time or the time at which velocity is equal to 10% of the peak velocity for this pulse [37]. Two soil categories are used in the analysis of Bray and Rodriguez-Marek [37]: (a) rock/shallow stiff soil (0–20 m of soil or weathered rock over competent rock with no soil having shear wave velocity $V_S < 180$ m/s) and (b) soil (mostly stiff soil $V_S > 180$ m/s). Soil conditions that are equivalent to USGS Class B and C have been selected, since the records corresponding to rock conditions according to USGS (Class A) are limited [25]. For each value of earthquake magnitude M the mean value, the mean plus two standard deviations value, $+2\sigma_{total}$, and the mean minus two standard deviations value, $-2\sigma_{total}$, are also calculated. According to the sample of seismic records used in this study, the dominant velocity period $T_{d\text{-}p}$ can be calculated with acceptable accuracy from Eq. (5) in the range of $+2\sigma_{total}$ and $-2\sigma_{total}$ standard deviations, for all the seismic magnitudes examined.

It should be noted that the $T_{d\text{-}p}$ period indicates the period of maximum spectral displacement. Thus, a region of constant spectral displacements should include periods that are both greater and smaller than $T_{d\text{-}p}$. Thus, in general, for the characteristic values T_D and T_E that define the constant spectral displacement region according to EC8 $T_D < T_{d\text{-}p} < T_E$. According to EC8 for greater magnitude earthquakes with $M_S > 5.5$ for which the Type 1 spectrum applies the transition period is T_D=2.0 s, while for the Type 2 spectrum ($M_S \leq 5.5$) the transition period is T_D=1.2 s, regardless of the soil category. From Fig. 3 it is clear that for the small-to-medium earthquake magnitude near-fault events that have been examined these values for corner periods might not be suitable. For seismic events with $M_W > 5.5$, there are only 9 from 52 records that have dominant period $T_{d\text{-}p} > T_D$=2.0 s. It is evident that the characteristic period T_D should be correlated with the seismic magnitude. The period T_E that marks the end of the constant spectral displacement region appears to be suitable for the whole range of M_W; however, the displacement sensitive region may be "narrower" depending on seismic magnitude.

In Figs. 4 and 5 the standard displacement spectra and the bi-normalized displacement spectra in terms of peak ground displacement $d_{g,max}$ and dominant period $T_{d\text{-}p}$ are shown, respectively, for damping ratio ξ=0%. The records are divided into four categories according to the moment magnitude: (a) 4.9 < M_W < 5.4, (b) 5.5 < M_W < 5.9, (c) 6.0 < M_W < 6.4 and (d) M_W > 6.5. Notice that in the analysis development the moment magnitude M_W has been used instead of the surface magnitude M_S, as the former is available from the databases used in this study. Small differentiation is expected in these two scales according to Wells and Coppersmith [44].

It is evident from Fig. 4 that the spectra present significant dispersion regarding the corner periods of the constant spectral displacement region. This differentiation diminishes when the periods are normalized according to the dominant period $T_{d\text{-}p}$ in Fig. 5. In Fig. 4 the mean spectra are drawn with a continuous line, while the displacement spectra according to the predictive models of Akkar and Bommer [23] and Cauzzi and Faccioli [24] are drawn with dotted lines. The available predictive models might underestimate spectral values in the near-fault area. An accurate estimation of earthquake magnitude, soil conditions and distance is needed for a more reliable prediction.

Notice that the bi-normalized spectra in Fig. 5 are characterized by a distinct peak around the dominant period $T_{d\text{-}p}$. The constant spectral displacement region extends around the dominant period $T_{d\text{-}p}$. Large amplification factors SD/d_{gmax} are usually related to records with low amplitude and large number of strong motion cycles, typical for backward directivity in the near-fault area. An average amplification factor $SD(T_{\text{d-p}}, \xi$=0%)$/d_{gmax} \approx 6.0$ corresponding to the dominant period $T_{d\text{-}p}$ is applicable for all magnitude

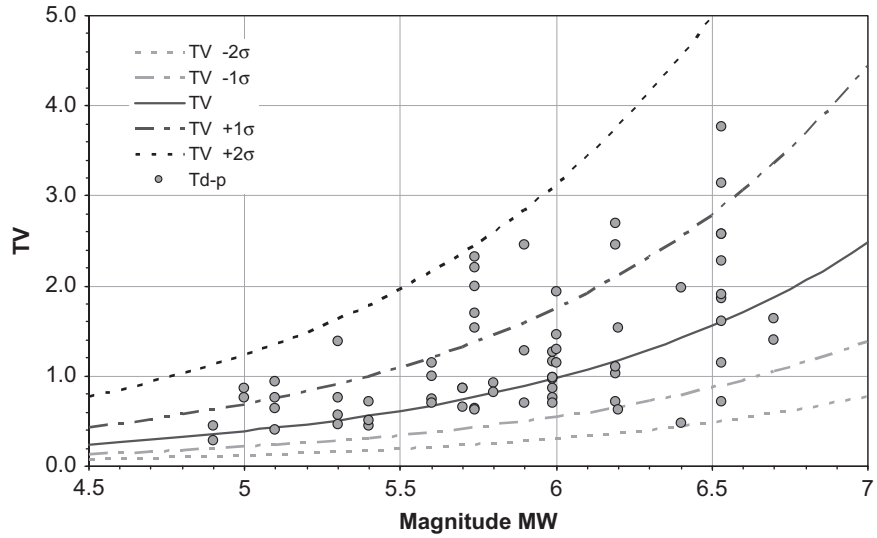

Fig. 3. Comparison of the dominant period of ground velocity $T_{d\text{-}p}$ for the near-fault records of Table 1 with the period T_V derived by Eq. (5) for the velocity pulse period.

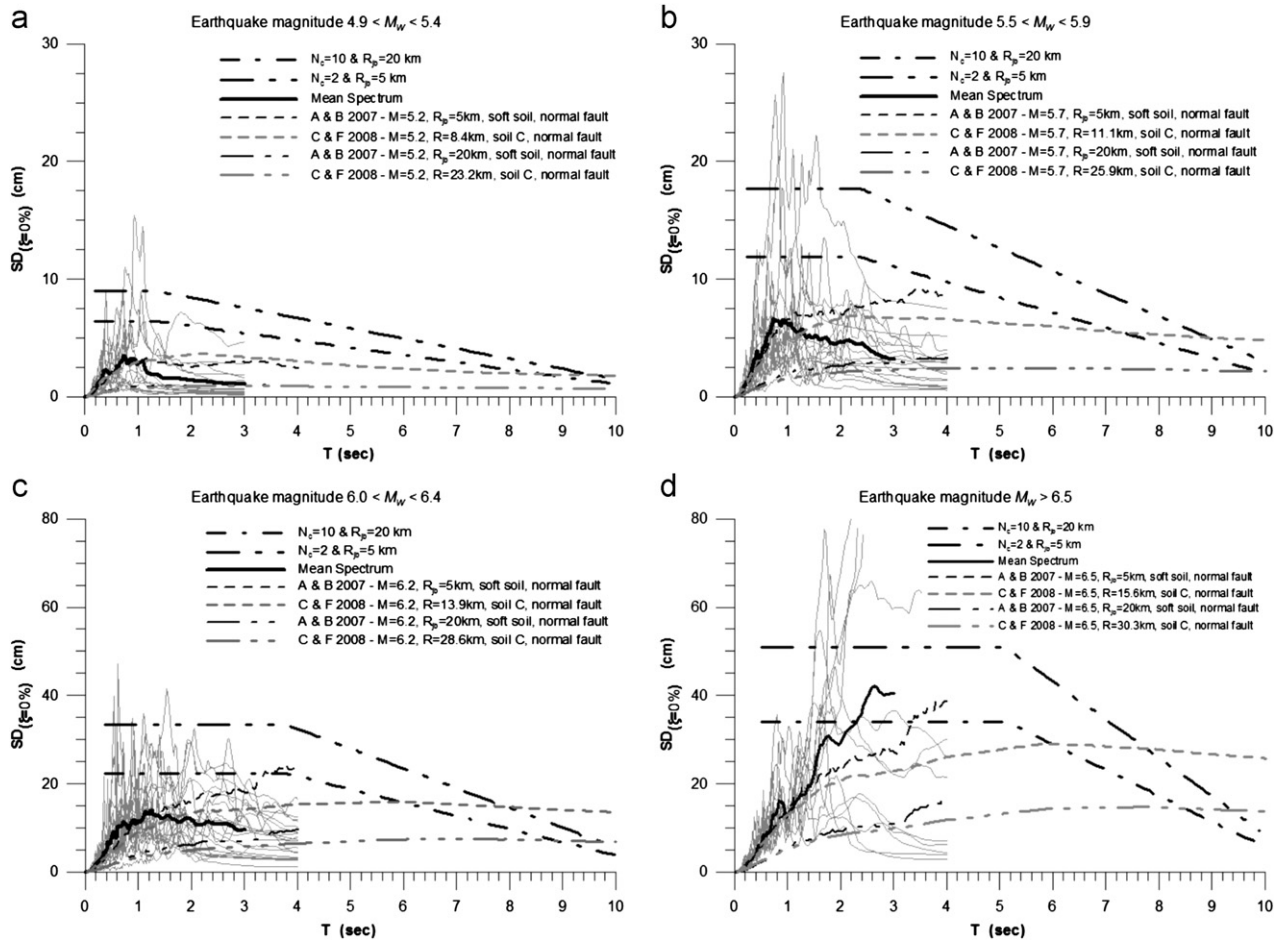

Fig. 4. Standard response spectra for near-fault earthquake records with magnitude (a) $4.9 < M_W < 5.4$, (b) $5.5 < M_W < 5.9$, (c) $6.0 < M_W < 6.4$ and (d) $M_W > 6.5$.

ranges, while the shape of the bi-normalized spectrum shown in Fig. 5 remains practically invariable for all magnitudes $M > 5.50$.

It should be noted that in the evaluation of the mean displacement response spectra for the near-fault region, the peak strong motion amplitude, which corresponds to a short duration motion at the forward directivity direction, should not be combined with the maximum spectral amplification coefficient, which corresponds to a long duration motion with large number of significant cycles usually recorded at the backward directivity direction. In that case an unrealistic displacement response spectrum would result in terms of spectral amplitude. Consequently, the number of cycles of motion should be considered as a critical parameter to determine the response spectra at a small distance from the causative fault.

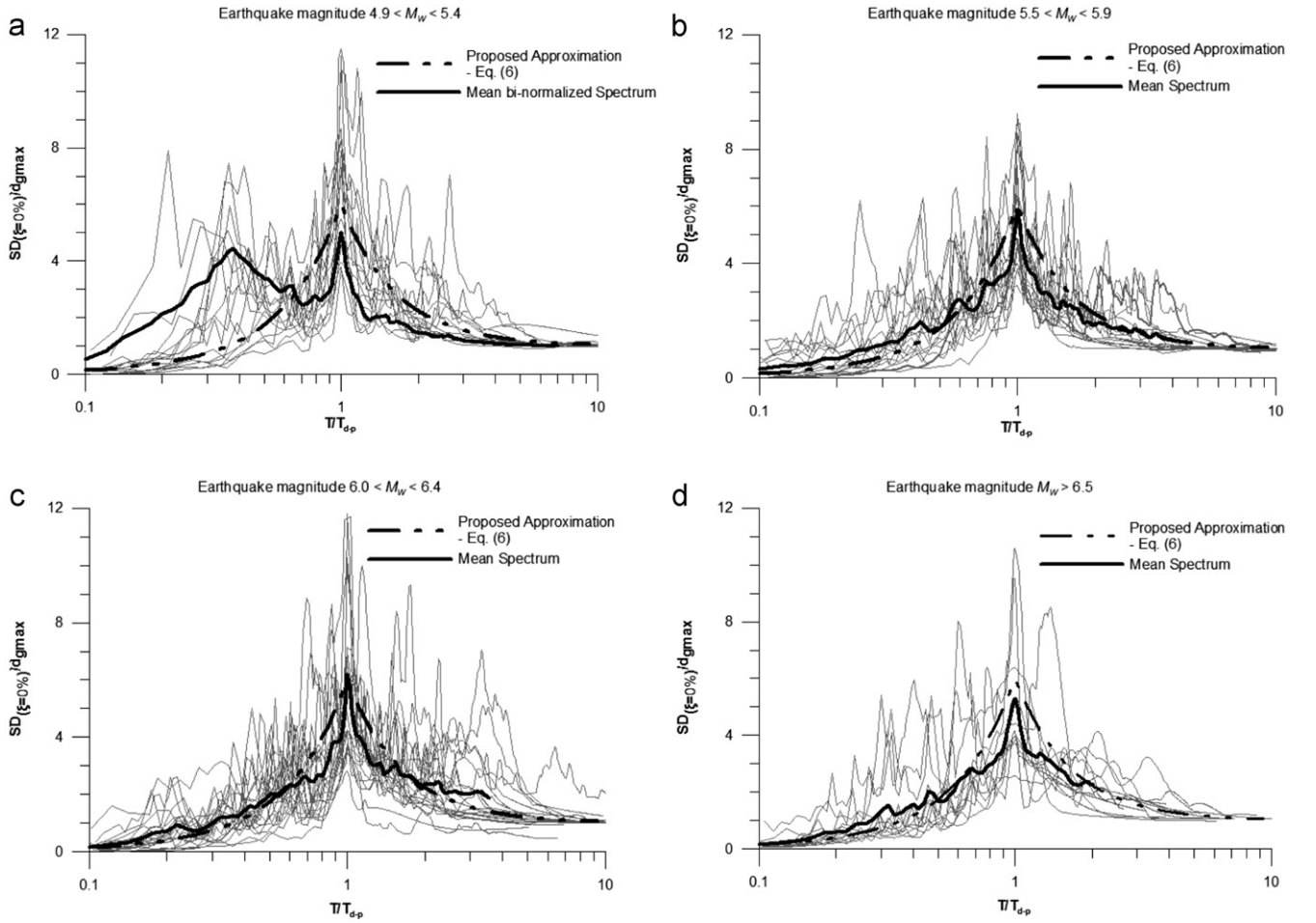

Fig. 5. Bi-normalized response spectra in terms of peak ground displacement $d_{g,max}$ and dominant period $T_{d\text{-}p}$ for all magnitude categories and proposed approximation using Eq. (6).

For a number of earthquake records, as shown in Table 1, a similarity between the periods $T_{v\text{-}p}$ and $T_{d\text{-}p}$ is observed. This similarity should be considered as rational mainly for the following two reasons:

1. For relatively small earthquake magnitudes, the dominant period $T_{d\text{-}p}$ is small enough to approach or even to be located in the velocity sensitive region of the response spectrum. This possibility increases for loose soil conditions, which lead to spectral amplification at higher periods. A characteristic example of this case is the PYR19306 record of 1993 Pyrgos, Greece, M_W=4.9 earthquake obtained at Soil Type C, as shown in Fig. 6(a) and (b), for which the two periods are identical; $T_{d\text{-}p}=T_{v\text{-}p}=0.28$ s.
2. For large earthquake magnitude, the directivity pulse becomes distinct in the acceleration time history, thus, dominating in the velocity response spectrum. A typical example is the LEF10301 time history of 2003 Lefkada earthquake, with M_W=6.2 recorded at Class C soil conditions shown in Fig. 6(a) and (b) with $T_{d\text{-}p}=T_{v\text{-}p}=0.62$ s. For this earthquake event a spectral amplification due to loose soil conditions in the period range between T=0.30 s and 0.70 s has been detected by applying deconvolution of the dynamic behavior of soil profiles to obtain the strong motion in the rock outcrop [45]. The possible coincidence of $T_{d\text{-}p}$ and $T_{v\text{-}p}$ periods strongly depends on the high frequency content of the velocity time history and soil characteristics; when either the record of strong motion is recorded on stiff soil formations or the motion is characterized by a profound high frequency content, the velocity pulse period $T_{d\text{-}p}$ increases and is expected to be significantly different from $T_{v\text{-}p}$.

When the $T_{d\text{-}p}$ and $T_{v\text{-}p}$ periods coincide, the velocity and displacement sensitive regions have no clear boundaries. For the determination of the constant spectral displacement region, the characteristic period T_D will be found in the region of constant spectral velocity.

To further evaluate the adequacy of the current Type 1 design displacement spectrum of Eurocode 8, the normalized displacement spectra in terms of the maximum ground displacement $d_{g,max}$ for magnitudes $M_W > 5.5$ and soil class B and C, respectively, are presented in Fig. 7(a) and (b) together with the mean displacement spectrum for each category and the corresponding EC8 spectrum. The spectral amplitude of the Eurocode design spectrum demonstrates a good average growth and spectral shape for both soil types. For short periods the EC8 spectrum seems to underestimate the spectral values for the examined near-fault records. A significant difference is noticed regarding the characteristic periods, which according to the selected sample of records, should be shifted to shorter periods. However, observations on spectral characteristics at large periods might be attributed to the filters applied for the correction of strong ground motion. The spectral amplification coefficient is in the range 3.60 for both soil categories.

In Figs. 8 and 9 the standard and the bi-normalized displacement spectra in terms of the maximum ground displacement $d_{g,max}$ are

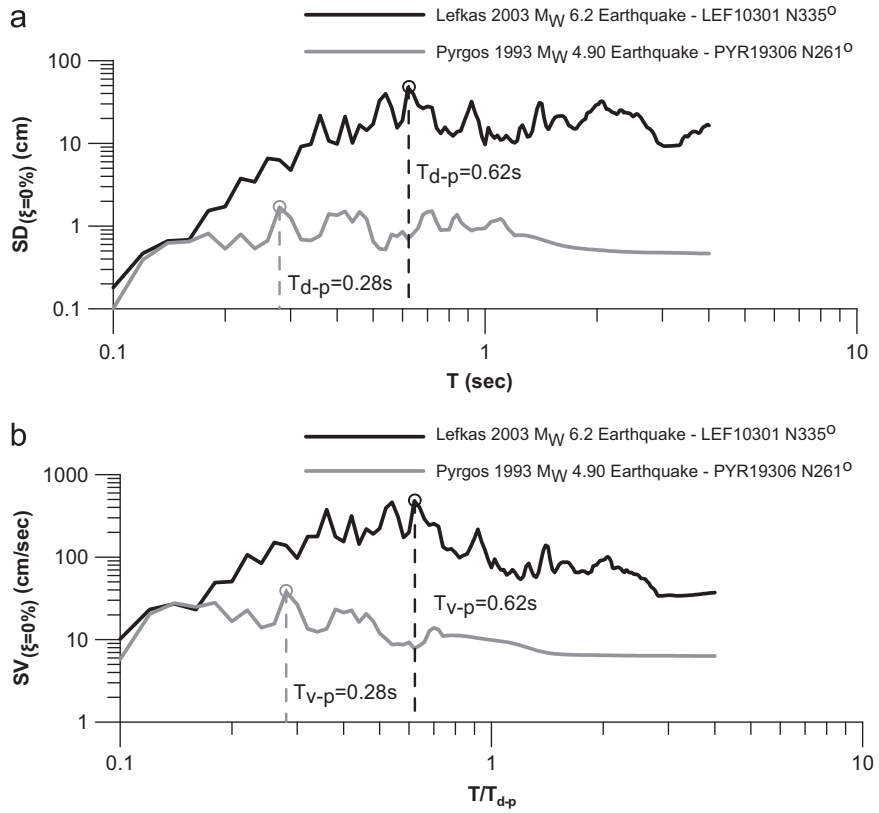

Fig. 6. PYR19306 record of 1993 Pyrgos Greece earthquake, with M_W=4.9 at Soil Type C and LEF10301 record of 2003 Lefkada Greece earthquake, with M_W=6.2 at Soil Type C: (a) displacement response spectra for zero damping ξ=0% and (b) velocity response spectra for zero damping ξ=0%.

shown for soil class B and C, respectively, for $M_W > 5.5$. The average value of M_W and indicative values of distance have been selected. As shown from Figs. 8(a) and 9(a) the displacement sensitive region for the average spectrum seems to be shifted to a higher period range for looser soil conditions. This fact is strongly attributed to the earthquake magnitude associated with the records at soil class C of the Imperial Valley 1979 earthquake, which has a dominant period greater than 2.0 s. The available predictive models for spectral displacement appear to be sensitive on the determination of soil conditions, earthquake magnitude and distance, while almost a coincidence of the two predictive equations in the range $0\text{ s} < T < 4\text{ s}$ is achieved for "Akkar and Bommer's" [23] soft soil conditions and "Cauzzi and Faccioli's" [24] soil category C.

The bi-normalized displacement response spectra shown in Figs. 8(b) and 9(b) present a distinct peak in their dominant period. Notice that the maximum spectral amplitude for both soil categories is about six times greater than $d_{g,max}$. The normalization in terms of the dominant period considerably improves the dispersion of spectral values and leads to a significantly smoothed spectral shape. Similar observations have been reported in the literature for spectral acceleration [18]. There is a significant reduction in standard deviation values STDEV, obtained by normalization as shown in Figs. 8(c) and 9(c). The nearly constant shape of the bi-normalized spectrum that is unaffected by soil category and earthquake magnitude as shown in Figs. 5, 8(b) and 9(b) allows the derivation of an approximation for the bi-normalized spectrum with the proposed simple equations of the form

$$\frac{SD(T,\xi=0\%)}{d_{g\,max}} = \begin{cases} 5(T/T_{d-p})^2 + (T/T_{d-p}), & T \le T_{d-p} \\ 1 + \frac{5}{(T/T_{d-p})^2}, & T > T_{d-p} \end{cases} \quad (6)$$

Eq. (6) is plotted in Figs. 5, 8(b) and 9(b), which indicate that the proposed approximation appears to be rational. However, the applicability and the appropriateness of Eq. (6) should be re-evaluated based on a more extensive database. This evaluation is currently performed by the authors.

4.2. Determination of spectral amplitude

To define the displacement spectrum for near-fault motion, it is necessary to estimate both the frequency range where the spectral displacement can be considered as constant, and the amplitude of the spectrum. The amplitude definition presupposes the calculation of a peak ground response and an amplification coefficient. Since the ground displacement time history is considerably sensitive to the digitization and correction procedures, as already mentioned, the possibility to estimate the spectral amplitude through the peak ground velocity is examined in the following.

The peak horizontal ground velocity for near-fault earthquakes is a function of earthquake magnitude and distance from the source and can be estimated using appropriate attenuation relationships available in literature. The following relationship proposed by Bray and Rodriguez-Marek [37] is used for the $+2\sigma_{total}$ and $-2\sigma_{total}$ standard deviation values:

$$\ln(PHV) = 4.58 + 0.34M_W - 0.58\ln(R_{rup}^2 + 7^2) \quad (7)$$

where R_{rup} is the rupture distance, i.e., the closest distance to the fault plane. The standard error for soil conditions is σ_{total}=0.49. In Fig. 10(a), (b), (c), (d) and (e) the peak horizontal ground velocity (PHV) obtained from Eq. (7) is compared with the actual velocity for the 1966 Parkfield earthquake, the 1979 Coyote Lake earthquake, the 1979 Imperial Valley earthquake, the 1984 Morgan Hill earthquake and the 1987 Whittier Narrows earthquake, respectively. In each case the average value obtained from Eq. (7) leads to a reliable estimate of PHV.

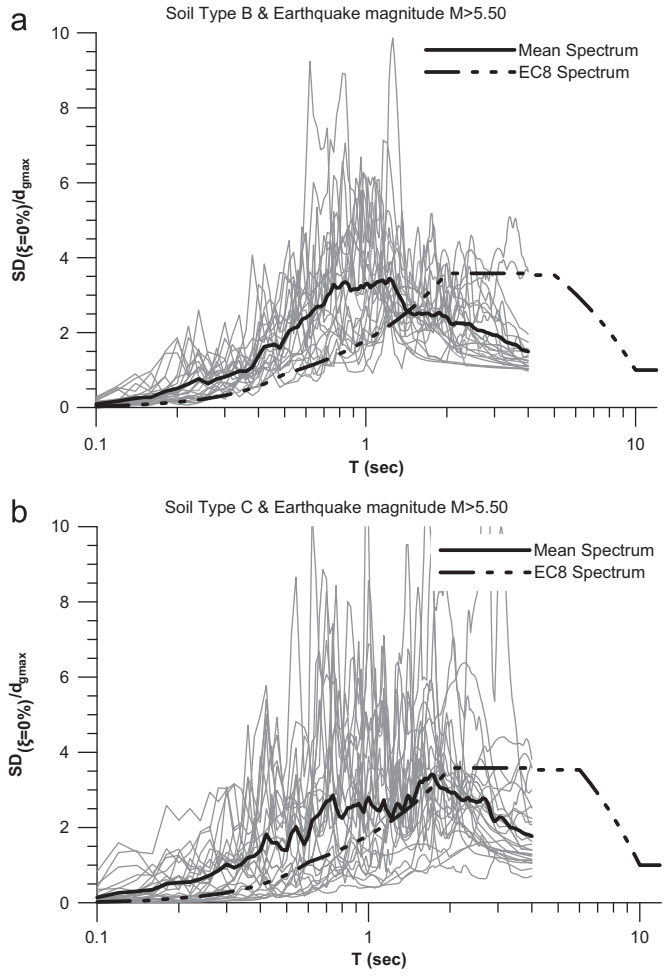

Fig. 7. Near-fault records with $M_W > 5.5$: (a) normalized displacement response spectra in terms of peak ground displacement d_{gmax}, for $\xi = 0\%$ and soil category B and (b) normalized displacement response spectra in terms of peak ground displacement d_{gmax}, for $\xi = 0\%$ and soil category C.

As presented in Taflampas et al. [46], a very good correlation exists between the ratio of spectral velocity SV($T_{d\text{-}p}$, $\xi = 5\%$) corresponding to the dominant period of motion to the effective velocity V_{mean} and the equivalent number of cycles of strong ground motion N_C. The N_C parameter is defined as the ratio

$$N_c = \frac{t_{bs}}{T_{d-p}} \tag{8}$$

where t_{bs} is the bracketed-significant duration related to the steep gradient of the time integral of the absolute velocity defined by the CAD index [47]:

$$CAD = \int_0^{t_r} |v_g| dt \tag{9}$$

and t_r is the total duration of motion. The t_{bs} duration is defined as the portion of strong motion that can produce spectral velocity values at least 90% of those of the original record. The bracketed-significant duration t_{bs} was found to be about 30% of the maximum ground velocity [46]. Effective velocity V_{mean} is the average velocity related to the t_{bs} duration and is calculated from the following expression:

$$V_{mean} = \frac{\int_{t_1}^{t_2} |v_g(t)| dt}{t_{bs}} \tag{10}$$

where t_1 and t_2 are the limits of the bracketed-significant duration t_{bs}. The following spectral amplification coefficient is evaluated for zero damping for the records of Table 1:

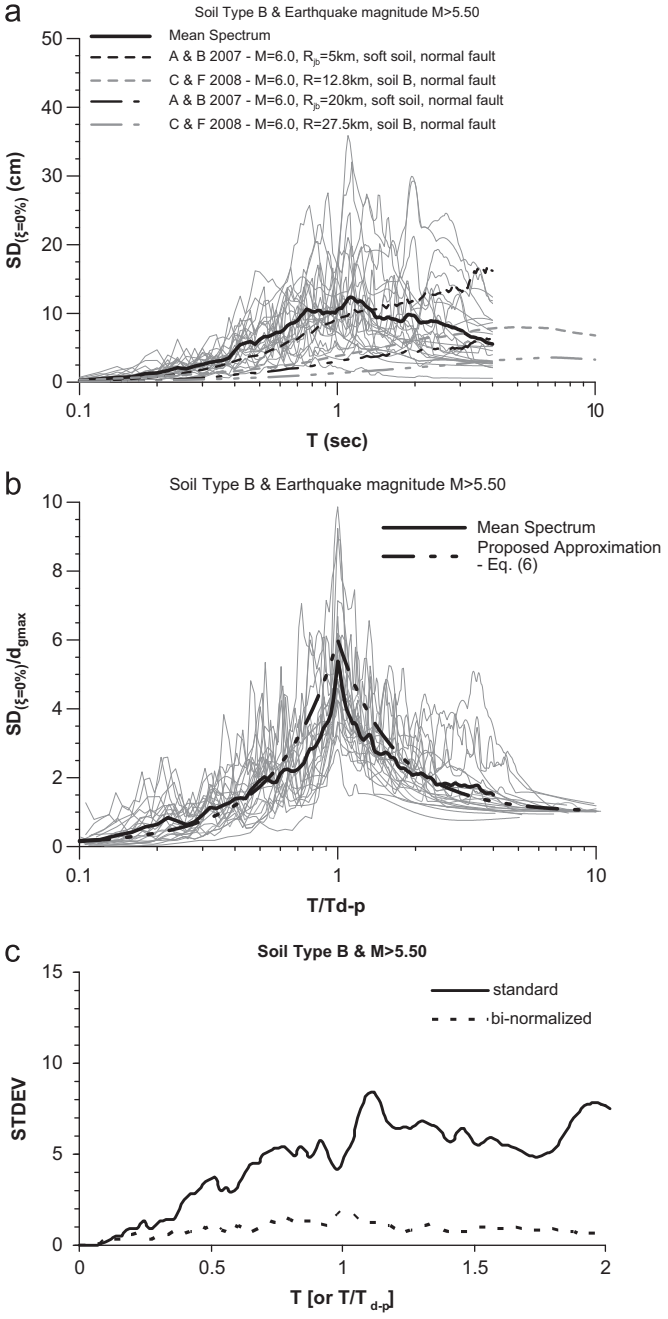

Fig. 8. Near-fault records with $M_W > 5.5$ and soil category B: (a) displacement response spectra for $\xi = 0\%$, (b) bi-normalized displacement response spectra in terms of peak ground displacement $d_{g,max}$ and dominant period $T_{d\text{-}p}$ for $\xi = 0\%$ and (c) standard deviation values for the mean standard (continuous line) and bi-normalized (dotted line) displacement response spectra for $\xi = 0\%$.

$$a_{v,T_{d-p}} = \frac{SV(T_{d-p}, \xi = 0\%)}{v_{mean}} \tag{11}$$

In Fig. 11 the parameter $a_{v,T_{d-p}}$ appears to be well correlated to the equivalent number of cycles N_C, with the following relationship:

$$\log(a_{v,T_{d-p}}) = 0.853 + 0.64\log(N_C) \tag{12}$$

thus, allowing the evaluation of the spectral amplification factor for zero damping from the expected number of cycles, which are related with the propagation of rupture in the near-fault.

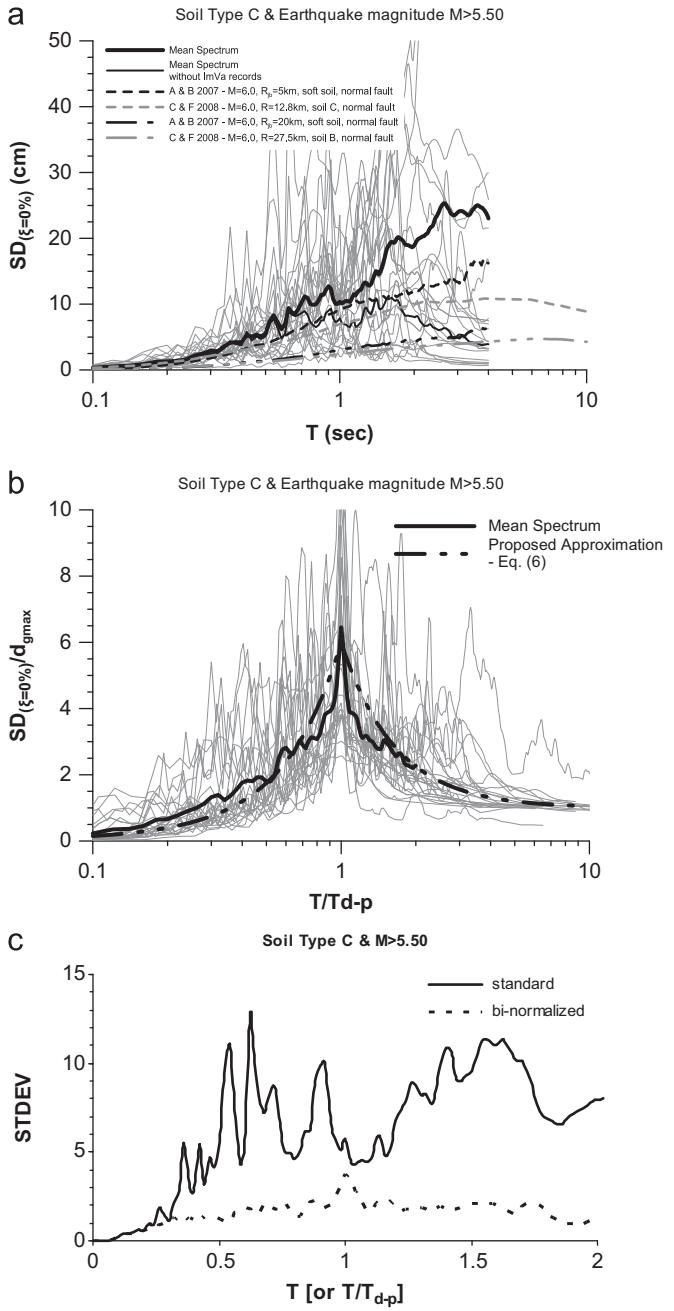

Fig. 9. Near-fault records with $M_W > 5.5$ and soil category C: (a) displacement response spectra for $\xi=0\%$, (b) bi-normalized displacement response spectra in terms of peak ground displacement $d_{g,max}$ and dominant period $T_{d\text{-}p}$ for $\xi=0\%$ and (c) standard deviation values for the mean standard (continuous line) and bi-normalized (dotted line) displacement response spectra for $\xi=0\%$.

Once an expected N_C is calculated, the amplification of the velocity spectrum in the dominant period can be obtained with reasonable accuracy. In order to calculate the maximum spectral displacement at the dominant period $T_{d\text{-}p}$, based on the well known relationship $SD=(T_{d\text{-}p}/2\pi)SV$, the effective velocity V_{mean} should be estimated. The trend of the V_{mean}/v_{gmax} ratio that shows a reduction with duration is also depicted in Fig. 12. Notice that a strong correlation of the ratio with N_C is not achieved. This reduction implies that for a large number of cycles, characteristic of backward directivity phenomena, the gradient of CAD integral becomes smoother and the effective velocity decreases. The bi-linear representation of the correlation shown in Fig. 12 with a discontinuous line is a conservative approach, whereby the effective velocity V_{mean} is 30% of the maximum ground velocity v_{gmax} for $N_C \geq 3$, while for lower number of cycles the V_{mean}/v_{gmax} ratio increases linearly. However, a more unbiased approach should use the curve drawn in Fig. 12.

The maximum ground velocity, v_{gmax}, can be estimated for the near fault region by applying the attenuation relationship of Bray and Rodriguez-Marek [37] given in Eq. (7).

5. Proposed methodology

Based on the previous observations and findings the following procedure is suggested to calculate the displacement spectra:

1. Estimation of the expected earthquake magnitude, M_W, based on the geometry and characteristics of the fault (deterministic) or from the historical seismicity of the site (probabilistic).
2. Calculation of the maximum ground velocity, v_{gmax}, based on the expected earthquake magnitude and the distance from the source using the average value of Eq. (7).
3. Estimation of the number of equivalent cycles N_C depending on the location of interest (at a distance and angle) in relation to the fault. When a strong forward directionality is expected $N_C=1$–3 can be selected. When no clear features of the fault are present two extreme scenarios can be considered, that is: (1) $N_C=2$ at $R_{jb}=5$ km and (2) $N_C=10$ at $R_{jb}=20$ km.
4. Calculation of V_{mean}/v_{gmax} ratio from the number of equivalent cycles N_c and Fig. 12.
5. Calculation of the spectral amplification coefficient $a_{v,T_{d-p}}=(SV(T_{d-p},\zeta=0\%)/v_{mean})$ from the number of equivalent cycles N_c and Eq. (11)—Fig. 11.
6. Calculation of the maximum spectral displacement SD_{max}, using the following relationship:

$$SD_{max}(T_{d-p},\zeta=0\%)=v_{g,max}(R,M_W)\frac{v_{mean}}{v_{gmax}}(N_c)a_{v,T_{d-p}}(N_c)\left(\frac{T_{d-p}}{2\pi}\right) \quad (13)$$

7. Determination of the frequency limits of the displacement sensitive region of the spectrum using Eq. (5), which provides the period T_V of the pulse with the largest amplitude that is expected to be equivalent to the dominant period $T_{d\text{-}p}$. The constant maximum spectral displacement region is established between the $+2\sigma_{total}$ and $-2\sigma_{total}$ standard deviation values of the dominant period. The inclusion of two standard deviations ensures that the peaks of SD spectra for all the magnitudes will be located in the region of constant spectral displacement, unlike the current design spectra, where the characteristic periods are practically independent of the earthquake magnitude. The start and end of the displacement sensitive region denoted by the corner periods T_D and T_E, respectively, can be determined using Eq. (5) as follows, for soil conditions:

$$\ln(T_D)=-5.60+0.93M_W-1.16 \quad (14a)$$

$$\ln(T_E)=-5.60+0.93M_W+1.16 \quad (14b)$$

For the four groups of seismic magnitudes defined earlier, namely: (a) $4.9<M_W<5.4$, (b) $5.5<M_W<5.9$, (c) $6.0<M_W<6.4$ and (d) $M_W>6.5$, and considering the average value for each range ($M_W=5.25$, 5.7, 6.2, 6.53), the displacement spectra are designed for the two extreme scenarios of step 3, namely: (1) $N_C=2$ at $R_{jb}=5$ km and (2) $N_C=10$ at $R_{jb}=20$ km. It should be noted that the steps 2–7 of the proposed methodology are based

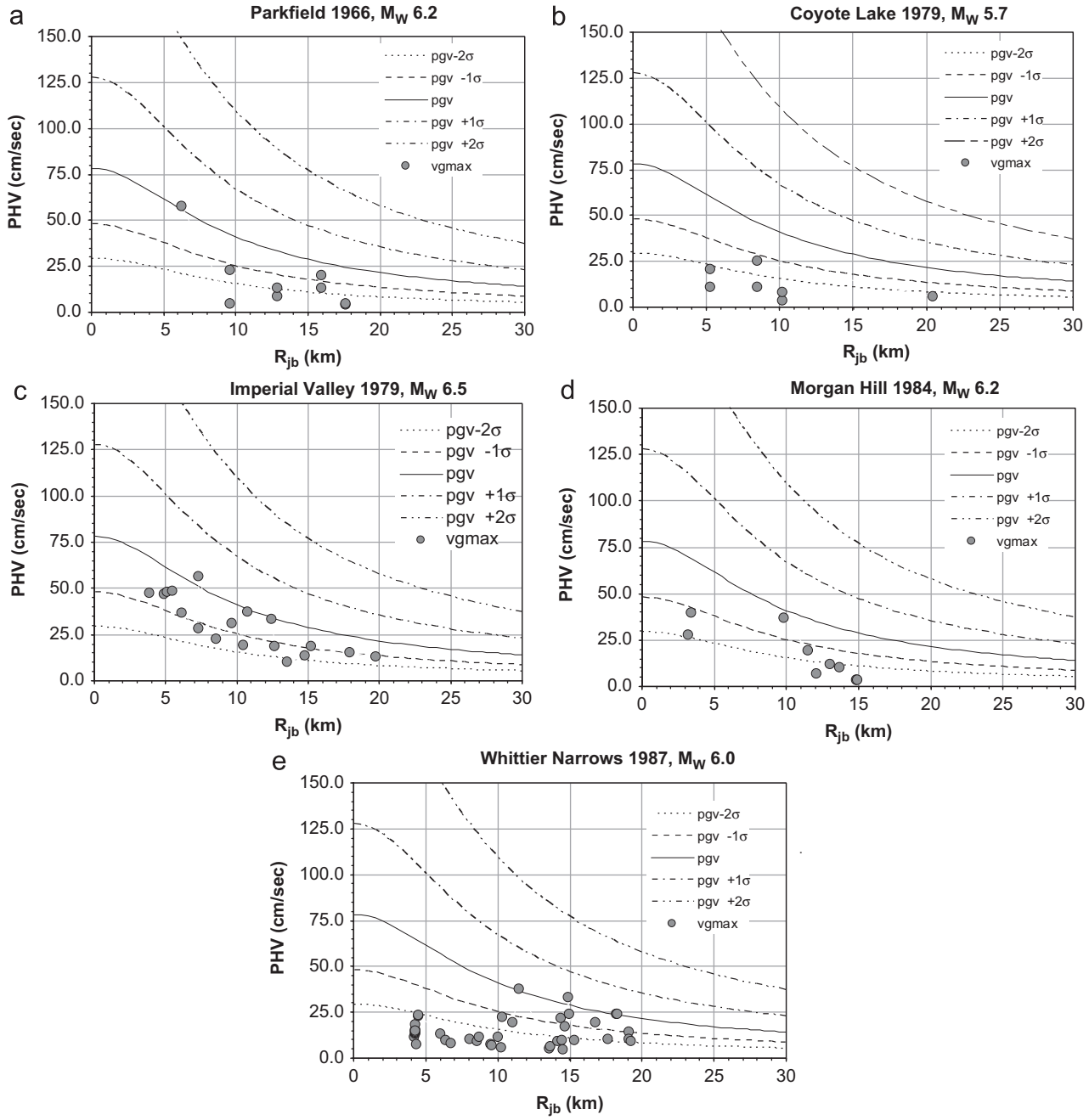

Fig. 10. Comparison of actual peak horizontal velocity, PHV, to the results of Eq. (7).

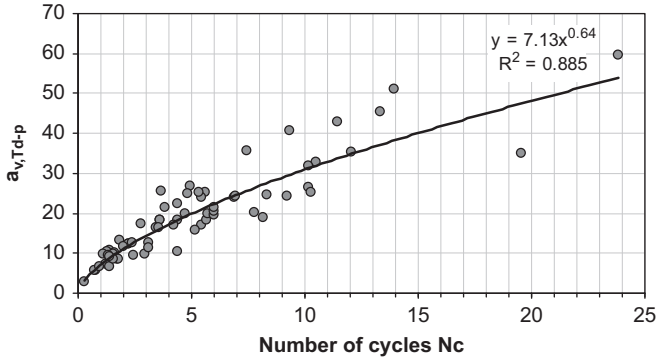

Fig. 11. Correlation of spectral amplification coefficient $a_{v,T_{d-p}}$ to the equivalent number of cycles N_C, for near-fault records.

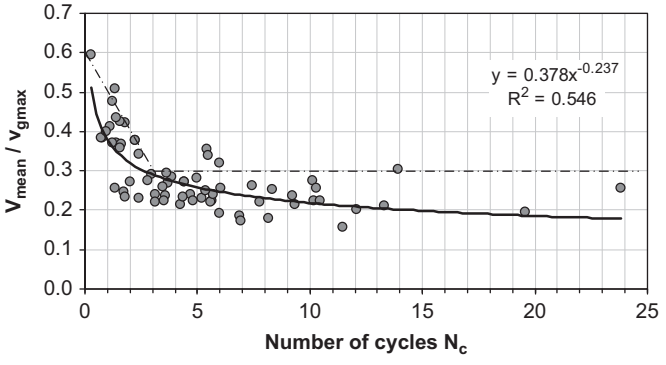

Fig. 12. Correlation of the V_{mean}/v_{gmax} ratio to the equivalent number of cycles N_C for near-fault records.

on relationships that include uncertainties, such as the estimation of normalized period. The significance of these uncertainties is an issue that will be assessed in a sequel study.

The resulting displacement spectra are compared with the displacement spectra and the bi-normalized displacement spectra, in terms of d_{gmax} and $T_{d\text{-}p}$, depicted in Fig. 4. It is noted that in each case the maximum displacement spectral region is well defined, while the proposed design spectrum ranges beyond the average spectrum for all levels of earthquake magnitude. The accuracy of the anticipated spectral displacements that result from the proposed methodology increases with the accuracy of the distance, seismic magnitude and estimated number of cycles. Notice that, as shown in Fig. 10, most of the PHV values are smaller than the mean value of Eq. (7); thus, the use of the average value results in higher spectral amplitude predictions, as shown in Fig. 4.

The above steps describe the procedure to create the displacement spectrum for zero damping $\xi=0\%$. In order to develop design spectra for damping ratios $\xi\neq 0\%$, one may apply Eq. (2) of EC8 [7].

A validation example of the proposed methodology is added using twelve records from the Athens 1999 M5.9 earthquake in Fig. 13. Values typical for the records used were applied, i.e, $N_C=2$ and 5, $R=17$ km and 20 km. It is shown that the methodology succeeds in identifying the displacement sensitive region of the average spectrum, yet the amplitude of the predicted spectrum is significantly greater than the average, because of the relatively small PHV values of the records. The approximation of the mean spectrum according to Eq. (6) appears to be valid.

The proposed methodology intends to provide a conservative, yet realistic, estimation for spectral displacements of near-fault records. The transformation to an acceleration spectrum using Eq. (1) might yield unusually high base shear coefficients for short-period structural systems. A different approach should be applied to evaluate the spectral acceleration of low period structures that might be based on the approximation of the bi-linear spectrum applying Eq. (6).

To assess the applicability of Eq. (2), the ratio of average spectral velocity for zero damping $SV_{(T,\xi=0\%)}$ to spectral velocity for $\xi=5\%$ $SV_{(T,\xi=5\%)}$ is drawn in Fig. 14(a) and compared with the corresponding value of Eq. (2) for $\xi=0\%$, that is, $\eta(0)=\sqrt{2}\approx 1.414$. From Fig. 14(a) it can be observed that in the period range $0.02\text{ s}<T<1.0\text{ s}$ the current damping correction factor expression leads to an underestimation of the zero damping spectrum for all the examined groups of earthquake magnitudes.

The normalization of periods to the dominant period, $T_{d\text{-}p}$, in Fig. 14(b) reveals an almost linear reduction trend of the $\eta_{(\xi=0\%)}=SV_{(T,\xi=0\%)}/SV_{(T,\xi=5\%)}$ ratio with the increase of $T/T_{d\text{-}p}$. In areas close to the dominant period for $0.8<T/T_{d\text{-}p}<1.2$, the $\eta_{(\xi=0\%)}$ coefficient is in the range of 2.5, as shown by the marked value in Fig. 14(b). The correlation factors shown in Fig. 14(b), which are greater than 80% for all magnitude groups, allow the development of an analytical equation that relates the $\eta_{(\xi=0\%)}$ coefficient with the normalized period $T/T_{d\text{-}p}$ and reveal the significant role of the dominant period $T_{d\text{-}p}$ on the response of elastic SDOF systems. The efficiency of damping in linearly elastic SDOF systems increases as their eigenperiod becomes smaller in comparison to the dominant period of the ground motion in the near-fault region for $\xi<5\%$. For the small-to-medium earthquake magnitude range $4.9<M_W<6.4$ the following relationship is proposed for near-fault excitations:

$$\begin{aligned}&\eta_{(T,\xi=0\%)}=-0.40\ln\left(\tfrac{T}{T_{d-p}}\right)+1.50 \quad \text{for } 0.1<\tfrac{T}{T_{d-p}}<0.8 \text{ or } 1.2<\tfrac{T}{T_{d-p}}<10\\ &\eta_{(T,\xi=0\%)}=2.5 \qquad\qquad\qquad\qquad \text{for } 0.8\le\tfrac{T}{T_{d-p}}\le 1.2\end{aligned} \tag{15}$$

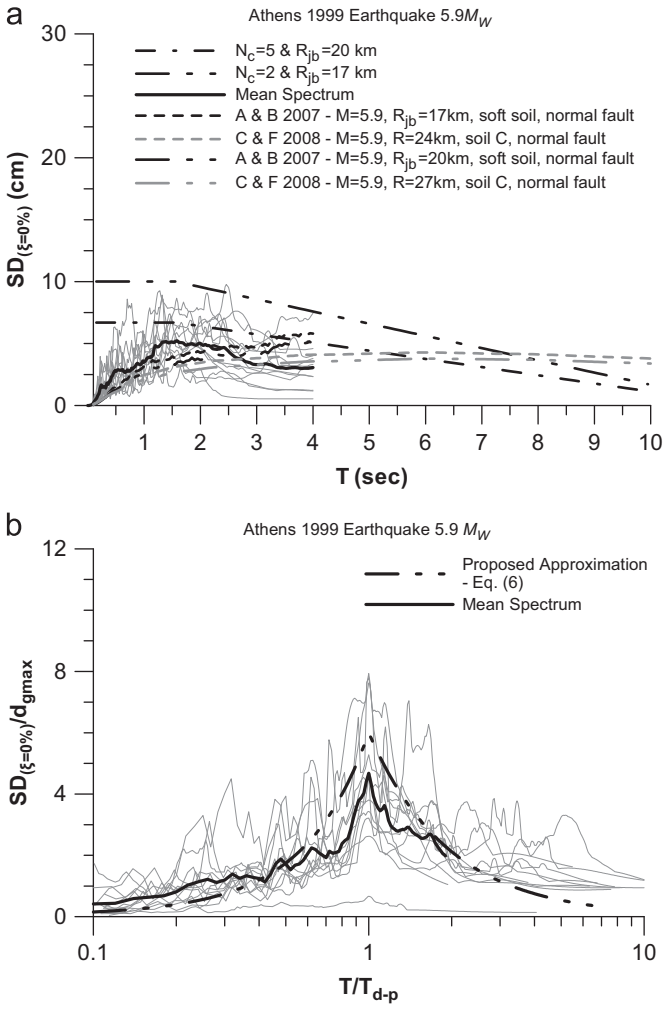

Fig. 13. Near-fault earthquake records of Athens 1999 M_W 5.9 earthquake records: (a) standard response spectra and (b) bi-normalized response spectra in terms of peak ground displacement $d_{g,max}$ and dominant period $T_{d\text{-}p}$.

Similar expressions can be derived for damping ratios $\xi=2\%$, 10%, 15% and 20%. The case of $\xi=20\%$ is shown in Fig. 15, where the application of a period independent value of $\eta(20)=0.632$ according to Eq. (2) appears to be unreliable for a significant range of periods. The $\eta(T,\xi)$ coefficient can be evaluated according to the following expression for $0.1\le(T/T_{d-p})\le 10$:

$$\begin{aligned}&\eta_{(T,\xi)}=c_1\ln\left(\tfrac{T}{T_{d-p}}\right)+c_2 \quad \text{for } 0.1<\tfrac{T}{T_{d-p}}<0.8 \text{ or } 1.2<\tfrac{T}{T_{d-p}}<10\\ &\eta_{(T,\xi)}=c_3 \qquad\qquad\qquad\qquad \text{for } 0.8\le\tfrac{T}{T_{d-p}}\le 1.2\end{aligned} \tag{16}$$

where the parameters c_1, c_2 and c_3 depend on the damping ratio ξ and are given in Table 2. For smaller normalized periods, i.e., $T/T_{d\text{-}p}<0.1$, the damping correction factor should linearly increase or reduce for $\xi>5\%$ or $\xi<5\%$, respectively, to reach $\eta=1$ for $T/T_{d\text{-}p}=0$ according to the theory of SDOF seismic response [48]. The dependence of η on the dominant period of motion and consequently on the magnitude of the earthquake is in accordance with what is mentioned in the most recent European predictive models for spectral displacement, i.e., [23,24].

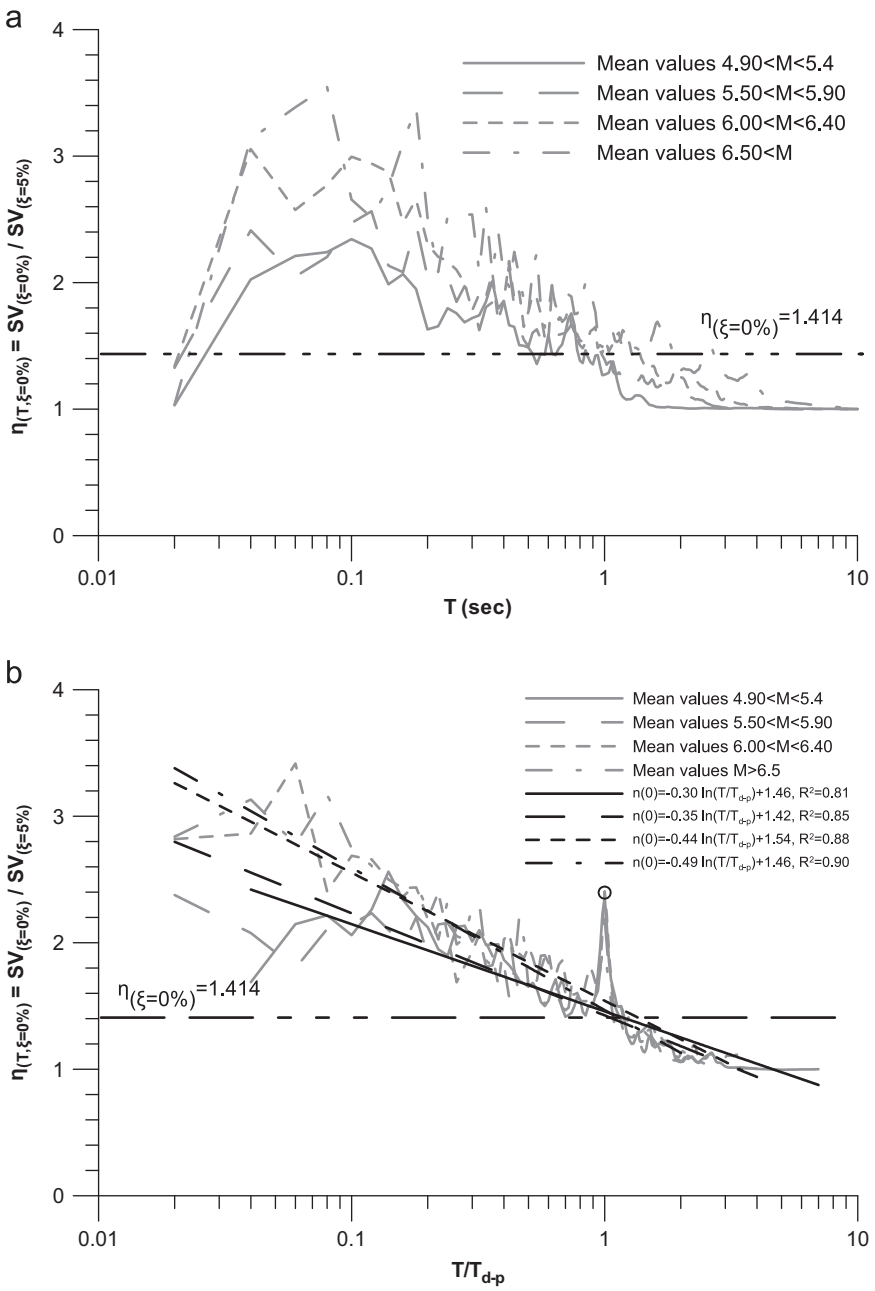

Fig. 14. Evaluation of damping correction factor η for average spectral values and $\xi=0\%$: (a) natural periods and (b) periods normalized by $T_{d\text{-}p}$.

6. Conclusions

In this study a new methodology to determine the elastic displacement spectrum for seismic design in the near fault region is presented. A sample of near-fault records is selected from small-to-medium magnitude earthquakes in order to be representative of the seismic activity in Europe. The displacement spectrum is determined in terms of moment magnitude and the type of directivity that controls the bracketed-significant duration t_{bs} of strong motion. Attenuation relationships for peak ground velocity available in literature and equations relating amplitude and duration are used to evaluate spectral amplitude. A discussion is made regarding the definitions available in literature for dominant period determination. Also an assessment of the current Eurocode 8 regarding displacement spectra is made. The following conclusions are drawn:

1. The amplitude of the *FSV* spectrum that corresponds to the harmonic component of $T_{d\text{-}p}$ cannot effectively represent a significant portion of the strong ground motion. A range of frequencies close to $1/T_{d\text{-}p}$ should be considered, even for the case of a distinct velocity pulse, a fact that justifies the applicability of the wavelet analysis in literature.
2. The dominant period of the pseudovelocity spectrum $T_{v\text{-}p}$ that is usually considered as the prevailing period of the velocity pulse can significantly underestimate $T_{d\text{-}p}$ especially as the seismic magnitude increases.
3. The corner periods T_D and T_E that define the start and end of the constant spectral displacement region according to EC8

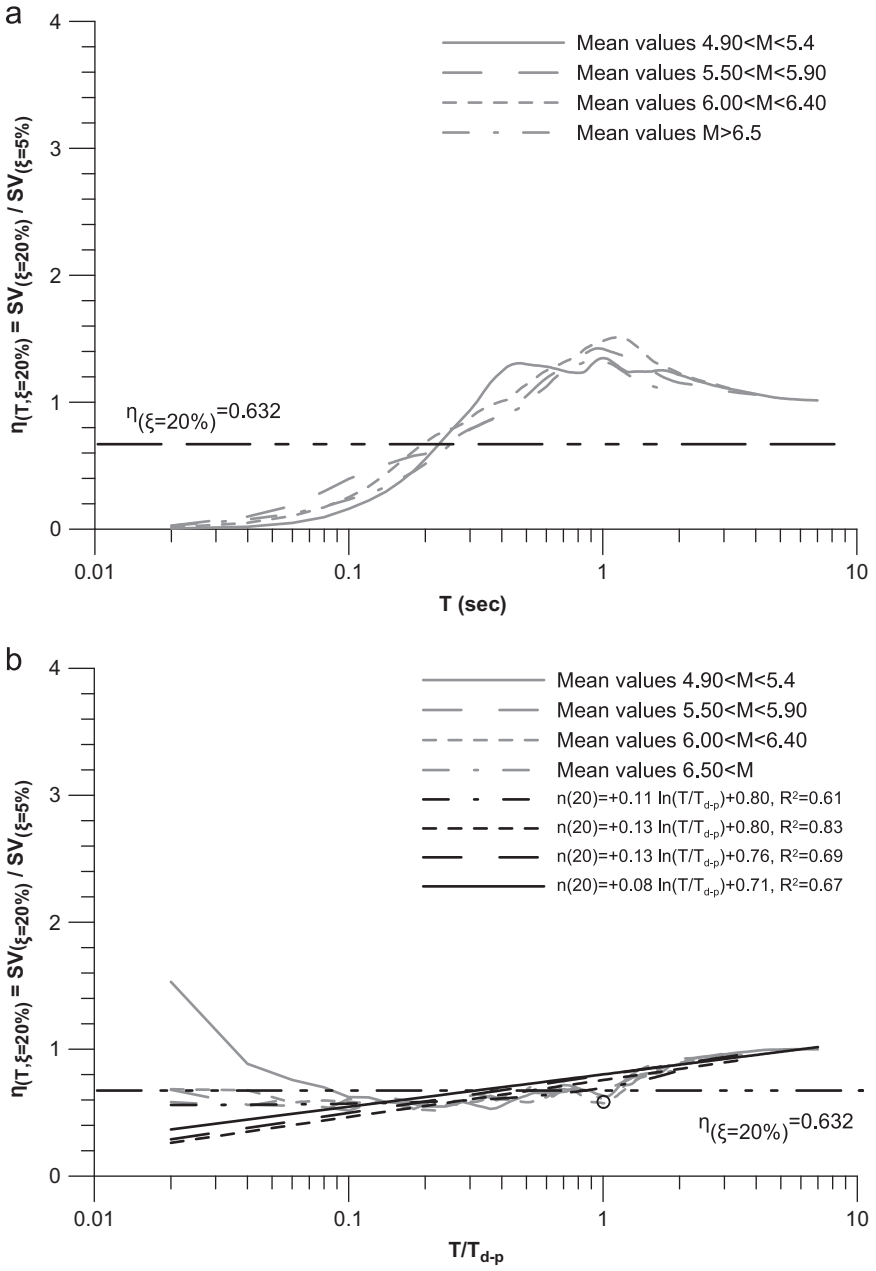

Fig. 15. Evaluation of damping correction factor $\eta_{(T,\xi)}$ for average spectral values and $\xi=20\%$: (a) natural periods and (b) periods normalized by $T_{d\text{-}p}$.

Table 2
Parameters for the evaluation of the damping coefficient $\eta(\xi)$ according to Eq. (16).

Damping coefficient ξ (%)	c_1	c_2	c_3
0	−0.40	1.50	2.5
2	−0.10	1.12	1.3
10	0.06	0.90	0.8
15	0.09	0.82	0.7
20	0.11	0.77	0.6

might be unsuitable for near-fault records and should be related to the earthquake magnitude. The determination of these periods in terms of the $T_{d\text{-}p}$ period is proposed using proper attenuation relationships available in literature.

4. The bi-normalization of the displacement spectra in terms of peak ground displacement $d_{g,max}$ and dominant period $T_{d\text{-}p}$ leads to a decrease of the dispersion of spectral values and smoothens the spectral shape, which is practically independent of soil category and earthquake magnitude. The bi-normalized spectrum presents a distinct peak at $T_{d\text{-}p}$, while the spectral amplification value related to this period is considerably greater than the values usually resulting from statistical analysis of large samples of displacement spectra.
5. The correlation between the spectral amplification related to $T_{d\text{-}p}$ and the equivalent number of cycles N_C already presented by the authors [46,47] is reconfirmed and used to determine the displacement spectra amplitude.
6. The proposed methodology effectively determines the displacement sensitive region of the response spectra in the small-to-moderate earthquake magnitude range.
7. A strong correlation between the normalized period $T/T_{d\text{-}p}$ and the damping correction factor η is detected, which implies that the efficiency of damping for linearly elastic systems is significantly affected by the ratio $T/T_{d\text{-}p}$. The proposed

relationship expressed by Eq. (15) allows modification of the proposed displacement spectra for different damping values, while the relationship proposed in EC8 for $\eta(\xi)$ is found to be unsuitable for a significant range of periods and damping values.

It should be stated that the methodology might not be applicable to all combinations of distance and magnitude since it is based on near-fault records. The applicability of EC8 provisions is assessed strictly for the near-source region. The results of the present research regarding the small frequency range could be re-evaluated based on digital records for which high cut-off frequency filters are not usually applied.

Acknowledgments

Diligent comments by anonymous referees led to significant improvement of this article. Dr. I. Taflampas, researcher at the Laboratory for Earthquake Engineering at National Technical University of Athens, has contributed in several phases of this research and his help is gratefully acknowledged. Insightful comments and discussions on strong motion correction procedures by Dr. N. Theodulidis, Research Director in the Institute of Engineering Seismology and Earthquake Engineering at Thessaloniki, helped to improve the development of this work.

References

[1] Heaton TH, Hall JF, Wald DJ, Halling MW. Response of high-rise and base-isolated buildings to a hypothetical M_W 7.0 blind thrust earthquake. Science 1995;267:206–11.
[2] Nakamura Y. Waveform and its analysis of the 1995 Hyogo-ken-Nanbu Earthquake. Report 23C. Tokyo, Japan: Railway Technical Research Institute; 1995.
[3] Erdik M. Report on 1999 Kocaeli and Düzce (Turkey) Earthquakes. In: Casciati F, Magonette G, editors. Structural control for civil and infrastructure engineering. World Scientific; 2001.
[4] Chen KC, Huang BS, Wang JH, Huang WG, Chang TM, Hwang RD, et al. Tsai CCP. An Observation of rupture pulses of the 20 September 1999 Chi-Chi, Taiwan, Earthquake from near-field seismograms. Bulletin of the Seismological Society of America 2001;91(5):1247–54.
[5] Priestley MJN, Calvi GM, Kowalsky MJ. Displacement based seismic design of structures. IUSS Press; 2007.
[6] Applied Technology Council. Seismic evaluation and retrofit of concrete building. ATC-40, Redwood City, CA, 1996.
[7] CEN—Comité Européen de Normalisation. Eurocode 8: design of structures for earthquake resistance. Part 1: general rules, seismic actions and rules for buildings. European Standard EN 1998-1, 2004.
[8] Rey J, Faccioli E, Bommer JJ. Derivation of design soil coefficients (S) and response spectral shapes for Eurocode 8 using the European strong-motion database. Journal of Seismology 2002;6(4):547–55.
[9] Pousse G, Berge-Thierry C, Bonilla LF, Bard P-Y. Eurocode 8 design response spectra evaluation using the K-net Japanese database. Journal of Earthquake Engineering 2005;9(4):547–74.
[10] Bommer JJ, Elnashai AS. Displacement spectra for seismic design. Journal of Earthquake Engineering 1999;3(1):1–32.
[11] Tolis SV, Faccioli E. Displacement design spectra. Journal of Earthquake Engineering 1999;3(1):107–25.
[12] Bommer JJ, Elnashai AS, Weir AG. Compatible acceleration and displacement spectra for seismic design codes. In: Proceedings of the 12th world conference on earthquake engineering, Auckland, 2000.
[13] Karakostas CZ, Athanassiasou CJ, Kappos AJ, Lekidis VA. Site dependent design spectra and strength modification factors based on records from Greece. Soil Dynamics and Earthquake Engineering 2007;27:1012–27.
[14] Pitilakis K, Gazepis C, Anastasiadis A. Design response spectra and soil classification for seismic code provisions. In: Proceedings of the 13th WCEE, Vancouver, Canada, 2004.
[15] Pitilakis K, Manou D, Anastasiadis A. Displacement response spectra for different soil conditions. In: Proceedings of the special session on Geotechnical Aspects of Eurocode 8, organised by ERTC-12 at the XIV European conference on soil mechanics and geotechnical engineering, 24–27 September 2007, Madrid, Spain.
[16] Singh JP. Earthquake ground motions: implications for designing structures and reconciling structural damage. Earthquake Spectra 1985;1(2):239–70.
[17] Mavroeidis G, Papageorgiou A. A mathematical representation of near-fault ground motions. Bulletin of the Seismological Society of America 2003;93(3):1099–131.
[18] Ziotopoulou K, Gazetas G. Are current design spectra sufficient for soil–structure systems on soft soils? In: Fardis MN, editor. Advances in performance-based earthquake engineering. Geotechnical, geological, and earthquake engineering 13, 13. Springer Science+Business Media B.V.; 2010. p. 79–87.
[19] Mylonakis G, Gazetas G. Seismic soil–structure interaction: beneficial or detrimental? Journal of Earthquake Engineering 2000;4(3):277–301.
[20] Mavroeidis GP, Dong G, Papageorgiou AS. Near-fault ground motions, and the response of elastic and inelastic single-degree-of-freedom (SDOF) systems. Earthquake Engineering and Structural Dynamics 2004;33:1023–49.
[21] Xu L, Xie L. Bi-normalized response spectral characteristics of the 1999 Chi-Chi Earthquake. Earthquake Engineering and Engineering Vibration 2004;3(2):147–55.
[22] Faccioli E, Paolucci R, Rey J. Displacement spectra for long periods. Earthquake Spectra 2004;20(2):347–76.
[23] Akkar S, Bommer JJ. Prediction of elastic displacement response spectra in Europe and the Middle East. Earthquake Engineering and Structural Dynamics 2007;36:1275–301.
[24] Cauzzi C, Faccioli E. Broadband (0.05 to 20 s) prediction of displacement response spectra based on worldwide digital records. Journal of Seismology 2008;12:453–75.
[25] PEER Strong Motion Database. 〈http://www.peer.berkeley.edu〉; 2010.
[26] Theodulidis N, Kalogeras I, Papazachos C, Karastathis V, Margaris V, Ch Papaioannou, et al. HEAD v.10: a unified Hellenic Accelerogram Database. Seismological Research Letters 2004;75(1):36–45.
[27] Spyrakos CC, Maniatakis ChA, Taflambas J. Evaluation of near-source seismic records based on damage potential parameters. Case study: Greece. Soil Dynamics and Earthquake Engineering 2008;28(9):738–53.
[28] Somerville PG, Smith NF, Graves RW, Abrahamson NA. Modification of empirical strong ground motion attenuation relations to include the amplitude and duration effects of rupture directivity. Seismological Research Letters 1997;68(1):199–222.
[29] Margaris BN. New fast digitization and correction procedures of the Greek strong motion records. In: Proceedings of the XXIV general assembly of the European Seismology Commission, Athens, September 19–24, 1994, vol. 2, p. 779–86.
[30] Skarlatoudis AA, Papazachos CB, Margaris BN. Determination of noise spectra from strong motion data recorded in Greece. Journal of Seismology 2003;7:533–40.
[31] Margaris B, Skarlatoudis A, Savvaidis A, Theodoulidis N, Kalogeras I, Koutrakis S. Strong-motion networks in Greece and their efficient use in the derivation of regional ground-motion prediction models. In: Akkar DS, Gulkan P, Eck T, editors. Earthquake data in engineering seismology: Springer editions, vol. 14; 2011. p. 71–80.
[32] Somerville PG. New developments in seismic hazard estimation. In: Proceedings of the 6th international conference on seismic zonation (6ICSZ), Palm Springs, California, 2000.
[33] Somerville PG. Development of an improved representation of near fault ground motions. In: Proceedings of the SMIP98 seminar on utilization of strong motion data, California Strong Motion Instrumentation Program, Sacramento, CA, 1998.
[34] Krawinkler H, Alavi B. Development of improved design procedures for near-fault ground motions. In: Proceedings of the SMIP98 seminar on utilization of strong motion data, California Strong Motion Instrumentation Program, Oakland, CA, 1998.
[35] Sasani M, Bertero VV. Importance of severe pulse-type ground motion in performance-based engineering: historical and critical review. In: Proceedings of the 12th world conference on earthquake engineering, New Zealand, 2000.
[36] Makris N. Rigidity–plasticity–viscocity: can electrorheological dampers protect base-isolated structures from near-source ground motions. Earthquake Engineering and Structural Dynamics 1997;26:571–91.
[37] Bray JD, Rodriguez-Marek A. Characterisation of forward-directivity ground motions in the near-fault region. Soil Dynamics and Earthquake Engineering 2004;24:815–28.
[38] Baker JW. Quantitative classification of near-fault ground motions using wavelet analysis. Bulletin of the Seismological Society of America 2007;97(5):1486–501.
[39] Menun C, Fu Q. An analytical model for near-fault ground motions and the response of SDOF systems. In: Proceedings of the 7th US national conference on earthquake engineering. Boston, Massachusetts: Mira Digital Publishing; 2002. p. 00011.
[40] Akkar S, Yazgan U, Gulkan P. Drift estimates in frame buildings subjected to near-fault ground motions. Journal of Structural Engineering 2005;131(7):1014–24.
[41] Taflampas IM. Evaluation of strong ground motion in engineering seismology and seismic vulnerability of structures. PhD thesis, Department of Earthquake Engineering, NTU Athens, 2009 [in Greek].
[42] Hudson DE. Some problems in the application of spectrum techniques to strong motion earthquake analysis. Bulletin of the Seismological Society of America 1962;52:417–30.
[43] Mohraz B, Elghadamsi FE. Earthquake ground motion and response spectra. In: Naeim F, editor. The seismic design handbook. Van Nostrand Reinhold; 1989.
[44] Wells DL, Coppersmith KJ. New empirical relationships among magnitude, rupture length, rupture width, rupture area, and surface displacement. Bulletin of the Seismological Society of America 1994;84(4):974–1002.

[45] Anastasiadis A, Margaris V, Klimis N, Makra K, Pitilakis K. The Lefkas Earthquake (M=6.2, Aug.14, 2003): strong ground motion and valuation of the subsoil's impact. In: Proceedings of the fifth Hellenic conference in geotechnical and geo-environmental mechanics, Technical Chamber of Greece, Xanthi, 2006. p. 2134 [in Greek].

[46] Taflampas J, Spyrakos CC, Maniatakis ChA. A new definition of strong motion duration and related parameters affecting the response of medium–long period structures. In: Proceedings of the 14th world conference in earthquake engineering, Beijing, China, October 12–17, 2008. p. 03-01-0057.

[47] Taflampas IM, Spyrakos CC, Koutromanos IA. A new definition of strong duration and related parameters affecting the response of medium–long period structures. Soil Dynamics and Earthquake Engineering 2009;29:752–63.

[48] Chopra A. Dynamics of structures: theory and applications to earthquake engineering. 3rd ed. Pearson/Prentice Hall; 2007.